DETERMINATION OF METHANE HYDRATE STABILITY ZONES IN THE PRUDHOE BAY, KUPARUK RIVER, AND MILNE POINT UNITS ON THE NORTH SLOPE OF ALASKA

By

Jason V. Westervelt

RECOMMENDED:

Dr. Abhijit Y. Dandekar

Dr. Godwin A. Chukwu

Dr. Santanu Khataniar

Shirish L. Patil, Advisory Committee Chair

Head, Petroleum Engineering Department

APPROVED:

Sukumar Bandopadhyay
Dean, School of Mineral Engineering

Susan C. Henricks
Dean of the Graduate School

March 6, 2004
Date

DETERMINATION OF METHANE HYDRATE STABILITY ZONES IN THE PRUDHOE BAY, KUPARUK RIVER, AND MILNE POINT UNITS ON THE NORTH SLOPE OF ALASKA

A

THESIS

Presented to the Faculty of the University of Alaska

in Partial Fulfillment of the Requirements

for the Degree of

MASTER OF SCIENCE

By

Jason V. Westervelt, B.S.

Fairbanks, Alaska

May 2004

ABSTRACT

Estimates range from approximately 37 to 44 trillion cubic feet of in-place gas in methane hydrate from within the Eileen Trend of the Prudhoe Bay (PBU), Kuparuk River (KRU), and Milne Point (MPU) Units on the North Slope of Alaska (Collett, 1993). This study was based on measuring pressure and temperature conditions for hydrate dissociation. The results showed that the depth of the hydrate stability zone (HSZ) ranges from 585 to 780 meters. The results from this study also show that the HSZ in the Alaska North Slope (ANS) is thinning westward. This study also showed that the effect of formation brines typically found on the North Slope only affects the depth of the hydrate stability zone by 30 to 45 meters when a porous media is not present. Experiments carried out on a porous media sample provided by the Anadarko Corporation showed that the formation brines only affect the depth of the hydrate stability zone by 10 to 15 meters. Geothermal gradients, gas composition, and the type of porous media play the biggest role in the thickness of the HSZ. These variables are also the most important when determining the depth to the HSZ.

DISCLAIMER

ACKNOWLEDGEMENTS

I would like to thank my advisor, Shirish L. Patil and my co-advisor, Dr. Dandekar for their guidance and support throughout the course of this research. My sincere appreciation goes to my advisory committee members Dr. Chukwu and Dr. Khataniar for their guidance. I also wish to extend my appreciation to Robert Hunter, Project Manager for the BP Exploration (Alaska), Inc. – U.S. Department of Energy Collaborative Gas Hydrate Research Project DE-FC-01NT41332 and Dr. Timothy Collett, U.S. Geological Survey, for providing data from the Alaska North Slope when needed. I would also like to thank Phil Tsunemori who helped me with running experiments. Without all their help this thesis would not have been possible.

I would like to thank the Petroleum Development Laboratory, United States Department of Energy, and BP Exploration (Alaska), Inc. for providing the financial support to accomplish my goals and studies. I would also like to thank the Anadarko Corporation for providing the core samples from Hot Ice #1 well.

Thanks to all the professors and students in the petroleum engineering department for making my stay at University of Alaska Fairbanks a most memorable one. Without your support I would not be where I am at today, thanks again. Also I don't know how I would have survived the winters of Fairbanks!

Finally, I am very grateful for the support my parents have given me while pursuing my college education. I feel very lucky to have such loving parents that helped

me get by when things got tough and therefore I would like to dedicate this thesis to my parents.

TABLE OF CONTENTS

LIST OF TABLES

LIST OF FIGURES

NOMENCLATURE

WK-11	West Sak River Well #11
WK-14	West Sak River Well #14
Wk-17	West Sak River Well #17
NWEN	North West Eileen State Well #2
NHST	North Highland State Well #1
HSZ	Hydrate Stability Zone
ANS	Alaska North Slope
PBU	Prudhoe Bay Unit
KRU	Kuparuk River Unit
MPU	Milne Point Unit
P	Pressure $[kPa]$
T	Temperature $[K]$
Γ^*	Geothermal Gradient
q	Rate at which heat enters the base of the permafrost
w	(harmonic) mean thermal conductivity
Δp	Change in pressure (psia)
σ	Interfacial tension (dynes/cm)
k	Permeability (md)
ϕ	Porosity (fraction)

$\Delta\mu_w$	Difference in chemical potential between empty hydrate cage and aqueous phase in equilibrium with hydrate, and $\Delta\mu_w^0$, the one at standard state.
Δv_w^{liq}	Difference in mole volume between empty hydrate and the liquid.
Δh_w^{liq}	Difference in enthalpies between empty hydrate and the liquid.
v_i	Number of type *i* cavities per water molecule.
V_l	Mole volume of water.
γ_w	Activity coefficient of liquid water.
X_w	Molar fraction of water.
σ_{H-w}	Surface tension of hydrate-water interface.
θ	Porous host-water contact angle.
r	Pore radii.
R	Gas Constant
y_{ki}	The fractional occupation of cavity type *i* and Langmuir constants of the cavity *i* for gas *k*.
T_f	Temperature at formation.
T_0	Temperature at standard conditions.
T_q	Temperature at quadruple point.
P_l	Pressure on liquid phase.
P_g	Pressure on gas phase

CHAPTER ONE

INTRODUCTION

1.1 Importance of Gas Hydrates

Methane hydrates, commonly referred to as gas hydrates, are crystalline, ice-like mixture of natural gas and water. Methane hydrates are concentrated forms of natural gas that are stable at low temperatures and high pressures. Methane is the most abundant natural gas and therefore "gas hydrates" and "methane hydrates" will be used interchangeably in this study.

Gas hydrates have been confirmed or inferred in polar regions, along continental margins, and in deep sea sediments. Hydrates of natural gas contain approximately 15 mol percent methane and 85 mol percent of water. Thus, one volume of hydrate could contain approximately 160 to 180 volumes of natural gas at standard conditions (Godbole et al., 1988). Yousif and Sloan (1991) stated that one cubic meter of gas hydrate at standard conditions could yield a maximum of 184 cubic meters of natural gas. These ratios of gas hydrates to natural gas are substantial and enormous amounts of natural gas could be produced from gas hydrates. In order to prove the methane production potential from these gas hydrates extensive research has to be done.

A primary research focus is the extent of gas hydrates in the world. World estimates range from 100,000 to 300,000,000 trillion cubic feet (Collett, 2001). Yet very little information in known about their resource potential, as is evident with the varying estimates stated previously. With such a wide range, extensive analysis on the extent of

methane hydrates needs to be conducted in order to bring this resource to production. In any case, the amount of gas hydrate-bearing reservoirs may greatly exceed the volume of known conventional gas reserves. Collett (1998) has suggested the volume of a gas hydrate accumulation is dependent upon five reservoir parameters:

1.) Areal extent of the gas hydrate occurrences

2.) Reservoir thickness

3.) Sediment porosity

4.) Degree of gas hydrate saturation

5.) The hydrate gas yield volumetric parameter which defines how much free gas is stored within the gas hydrate, also know as the "hydrate number"

Understanding these parameters in detail will allow the development of different production schemes to bring this vast resource to the market. Currently there are only a few production schemes that can tap into this resource. The three most practical schemes are thermal stimulation, in which an external source of energy is used; depressurization, in which the pressure of an adjacent gas phase is lowered to cause decomposition; and inhibitor injection, in which methanol or some combination of inhibitors is used to disequilibrate the system (Youslf et al., 1991).

1.2 Objective of Study

The North Slope of Alaska has been producing oil and gas for nearly three decades. Currently these reserves have been on a rapid decline and with advancements in technology and new discoveries more of these reserves are being produced. With the depletion of these reserves, new reserves need to be discovered in order to meet energy demands. One new discovery that could fill the energy gap for years to come is the production of natural gas from gas hydrates. Figure 1.1 illustrates the effect that gas hydrates could have in helping to meet the gas demand for future years.

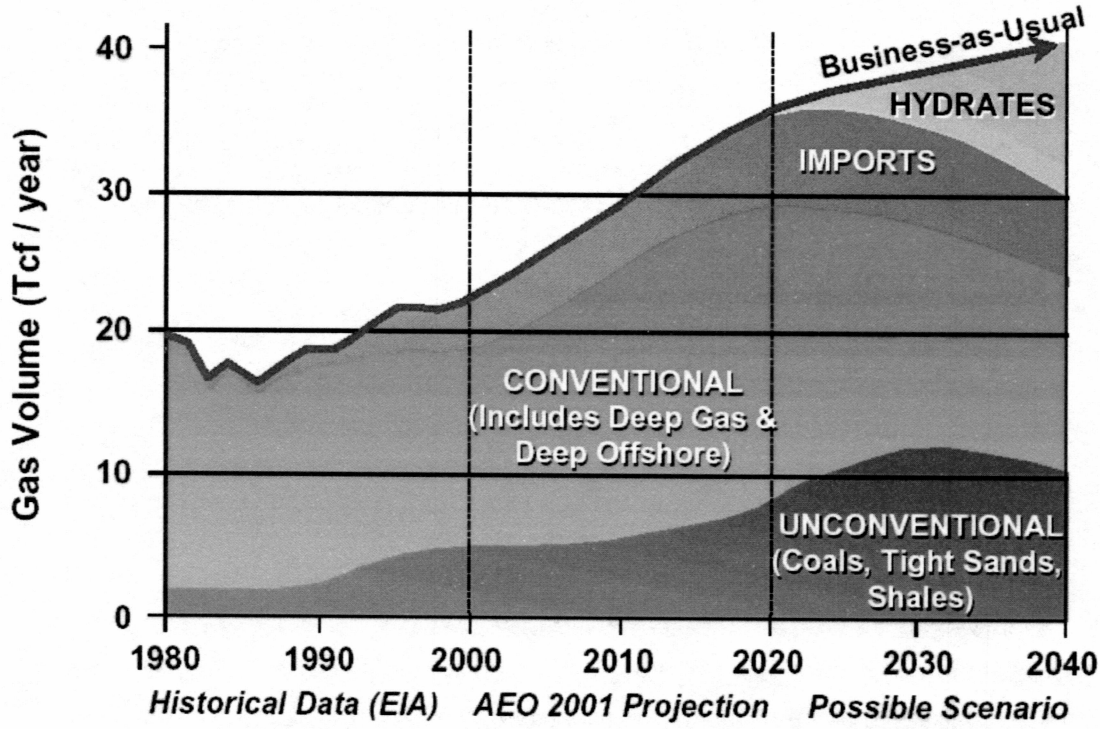

Figure 1.1: How Hydrates can Help Meet the Future Energy Demand (Courtesy: US Department of Energy)

Gas hydrates were first confirmed in 1972 on the North Slope of Alaska. A great advantage to making gas hydrates an economical resource is that the infrastructure already exists from decades of oil and gas production. Gas hydrates have been confirmed or inferred to occur in 50 North Slope exploration and production wells. In the Eileen Trend of the Prudhoe Bay, Kuparuk River, and Milne Point oil fields in northern Alaska, as much as 37 to 44 trillion cubic feet of in-place gas hydrates could exist (Collett, 1993). To bring this vast resource to production requires study of the Alaska North Slope (ANS) gas hydrate stability.

The primary objective of this work is to characterize the formation/dissociation of gas hydrates with and without the presence of porous media at or near reservoir conditions. Measurements are carried out in the presence of typical formation brines found in the Prudhoe Bay, Kuparuk River, and Milne Point Units on the North Slope of Alaska. The results along with geothermal gradients in the area are used to develop hydrate stability zones to determine the depth of hydrate stability. The design of gas hydrate production technology will require a thorough knowledge of the thermodynamic properties of gas hydrates under reservoir conditions. The experimental data obtained from this work will allow the hydrate stability zones of interest to be identified and possibly develop techniques for the safe production of natural gas from gas hydrates.

CHAPTER TWO

LITERATURE REVIEW

2.1 World Wide Occurrences

In recent years methane hydrates have been confirmed all over the world. There are typically three types of environments where hydrates accumulate. Hydrates can be found in arctic environments overlain by continuous permafrost, particularly the North Slope of Alaska, Northern Siberia, and Northern Canada. The other two environments where hydrates have been confirmed are in offshore continental margins and in deep marine sediments. The Gulf of Mexico, offshore Guatemala, offshore maritime Canada, and offshore Japan are typical areas where the pressure and temperature conditions are ideal for the formation of methane hydrates. These are just a few of the major areas where hydrates have accumulated. Figure 2.1 shows the locations of confirmed and inferred hydrate deposits thought out the world.

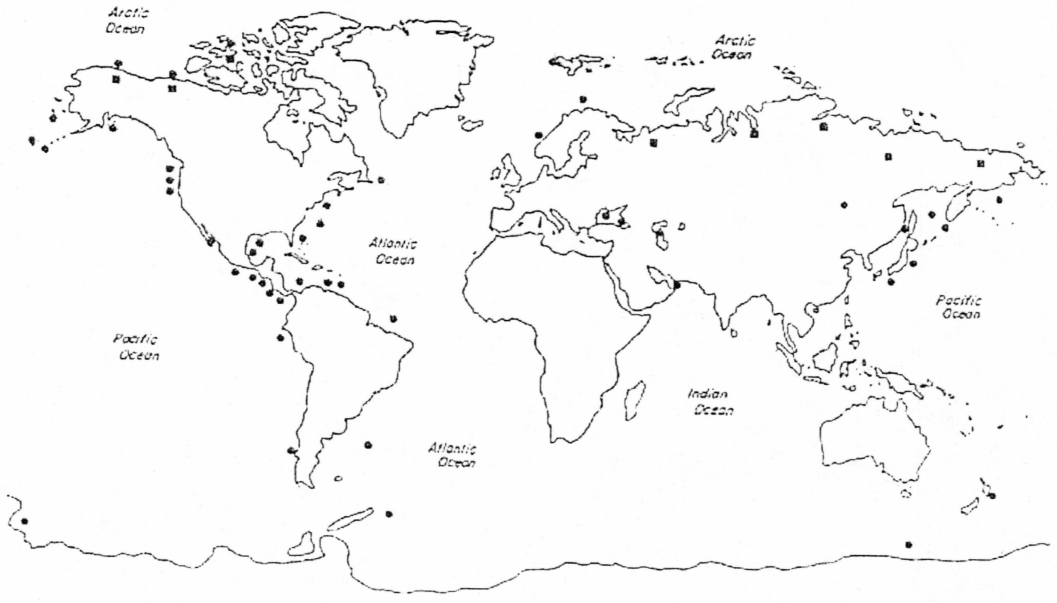

Figure 2.1: Locations of World Wide Occurrences (modified from Kvenvolden, 1988)

2.2 Gas Hydrate Estimates

Worldwide natural gas reserves are estimated at 13,000 trillion cubic feet. On the global scale, estimates of in-place gas hydrates range from 100,000 to almost 300,000,000 trillion cubic feet (Collett, 2001). These values range over three orders of magnitude, but in any case the potential natural gas hydrate resource exceeds the conventional gas reserves.

Estimates of gas hydrates in permafrost regions of the United States (i.e., Alaska) range from 11 trillion cubic feet to 25,000 trillion cubic feet, while estimates in oceanic sediments along the continental margins of the United States range from 2,680 trillion cubic feet to 6,710,000 trillion cubic feet (modified from Kvenvolden, 1998). Collett

(2001) states that nearly half of all gas hydrates resources in the United States are found in offshore Alaska.

On the North Slope of Alaska, Collett (1997) has estimated that there is approximately 590 trillion cubic feet of in-place gas within hydrates. Particularly in the Eileen Trend of the Prudhoe Bay, Kuparuk River, and Milne Point Units, estimates of natural gas from gas hydrates range from 37 to 44 trillion cubic feet (Collett, 1993). Figure 2.2 shows the aerial extent of gas hydrates and free gas found in the Prudhoe Bay (PBU), Kuparuk River (KRU), and the Milne Point Units (MPU) on the North Slope of Alaska.

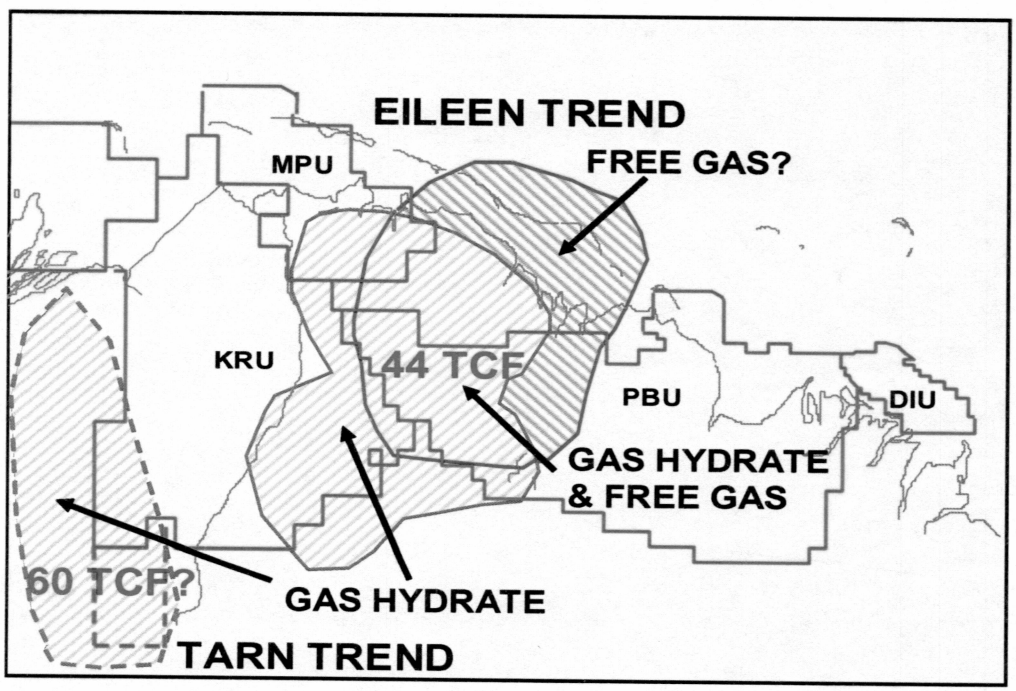

Figure 2.2: North Slope Occurrence of Gas Hydrates
(Courtesy: BP Exploration (Alaska), Inc. and the U.S. Geological Survey)

2.3 Historical Overview of Hydrates

In 1810, Sir Humphrey Davy first discovered hydrates while performing experiments with chlorine gas and water. He found that chlorine gas in water freezes more readily than pure water. Over the next century many researchers determined what compounds would form hydrates.

In 1934, Hammerschmidt showed that gas hydrates were responsible for plugging gas lines at temperatures above the ice point. This discovery caused a great interest in hydrate forming conditions. Many scientists began to look at variables such as pressure, temperature, composition, and phase behavior of hydrates.

In Russia, Makogon and co-workers announced in 1969 that methane hydrates were present in the permafrost in northern Siberia (Vasillev et al., 1970). A few years later Katz (1971) pointed out that the geologic conditions on the North Slope of Alaska were favorable for hydrate formation. On March 15, 1972, hydrates were confirmed on the North Slope of Alaska when Arco and Exxon recovered gas hydrate core samples in pressurized core barrels at several depths between 1893 and 2546 ft from the Northwest Eileen Well No. 2 in the Prudhoe Bay field (Kvenvolden and McMenamin, 1980). Also in 1972, gas hydrate was discovered in the Mackenzie Delta, Northwest Territories, Canada. In February and March of 1998, a 1150 m deep gas hydrate research well, JAPEX/JNOC/GCS Malik 2L-38, was completed at the northeastern edge of the Mackenzie Delta, Northwest Territories, Canada. Malik 2L-38 was the first research well to investigate natural hydrate occurrences beneath the permafrost (Dallimore et al., 1999).

On March 31, 2003 the Anadarko Corporation started drilling a research well (Hot Ice Well #1) targeting suspected gas hydrate-bearing reservoirs 80 miles south of Prudhoe Bay, south west of the Kuparuk field and west of the Alpine field. After 22 days of operation the drilling was suspended until winter. Anadarko completed drilling to a depth of 2,300, but apparently did not encounter significant gas hydrates. Anadarko had hoped to determine the extent of the hydrate gas resource in the area and to test its potential for production (Bradner, 2002).

2.4 The Structure of Gas Hydrates

Gas hydrates are solid structures that consist of water and gas molecules. These solid structures are known as clathrates. Clathrate comes from the Latin word meaning, "cage". The Collins English Dictionary defines clathrate as "a solid compound in which molecules of one substance are physically trapped in the crystal lattice of another". Water is the host molecule that forms the cage like structure due to the hydrogen bonding, whose voids the guest molecule penetrates. All molecules that fit into the cavities will be able to stabilize the host lattice, unless they show a specified chemical interaction with the solvent molecules (Van Der Waals and Platteeuw, 1959). Depending on the gas molecule, hydrates are characterized by three different crystal structures, cubic structure I, cubic structure II, and hexagonal structure H. The most common structures are cubic structure I and cubic structure II. These structures can be seen in Figures 2.3 and 2.4 respectively. Structure I gas hydrates is more commonly found in nature. These two structures represent different arrangements of water molecules resulting in slightly

different shapes, sizes, and assortments of cavities. Methane, ethane, and carbon dioxide typically form a structure I hydrate whereas propane and iso-butane commonly form structure II hydrates.

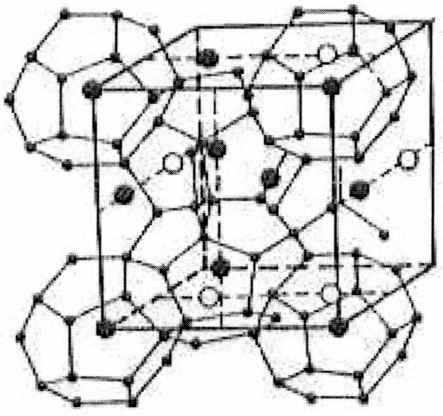

Figure 2.3 – Cubic Structure I

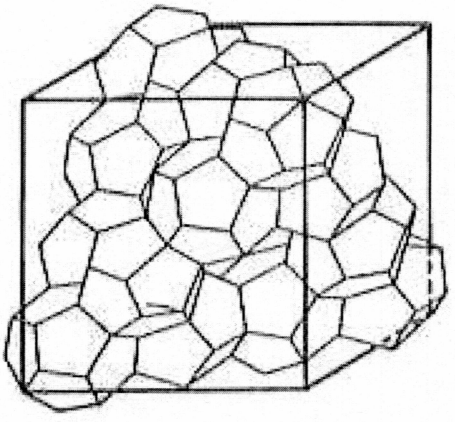

Figure 2.4 – Cubic Structure II

2.4.1 Cubic Structure I

A hydrate of structure I consists of 46 water molecules, which form two small dodecahedral voids and six large tetradecahedral voids. These small voids can only hold gas molecules with dimensions less then 5.2 angstroms and the large voids cannot exceed 5.9 angstroms. When a gas such as methane, whose molecular dimension does not exceed 5.2 angstroms, forms hydrates, both the

small and large voids can be completely filled. The chemical composition of a structure I methane hydrate can be expressed by Equation 1 (Makogon, 1981).

$$8CH_4 46H_2O \qquad (1)$$

2.4.2 Cubic Structure II

Gases with molecular dimensions in the range of 5.9 to 6.9 angstroms form structure II hydrates. Propane and iso-butane are two typical gases that form structure II hydrates. Structure II hydrates consists of 136 molecules of water with 16 small voids and eight large voids. The maximum diameter of the small voids is 4.8 angstroms, while the larger voids have a maximum diameter of 6.9 angstroms. The chemical composition of a structure II propane or isobutene hydrate is given by Equation 2 (Makogon, 1981).

$$8(C_3H_8, i\text{-}C_4H_{10})136H_2O \qquad (2)$$

2.4.3 Hexagonal Structure H

Structure H hydrates were first identified by Ripmeester and others (1987) in a laboratory while studying nuclear magnetic resonance spectroscopy together with X-Ray and power diffraction. Structure H hydrates are unique because a number of large molecules are able to fit into the largest voids of these hydrates.

These hydrates have cavities large enough to contain molecules the size of common components of naphtha and gasoline (Sloan, 2000).

2.5 Hydrate Thermodynamics

The thermodynamics of hydrates are characterized by P-T diagrams. These diagrams show the different phases that exist at different temperatures and pressures. Figure 2.5 shows the hydrate phase equilibrium for several components found in natural gas. At lower temperatures hydrocarbon gas, liquid water, hydrate, and ice are all in equilibrium whereas at higher temperatures ice is not present.

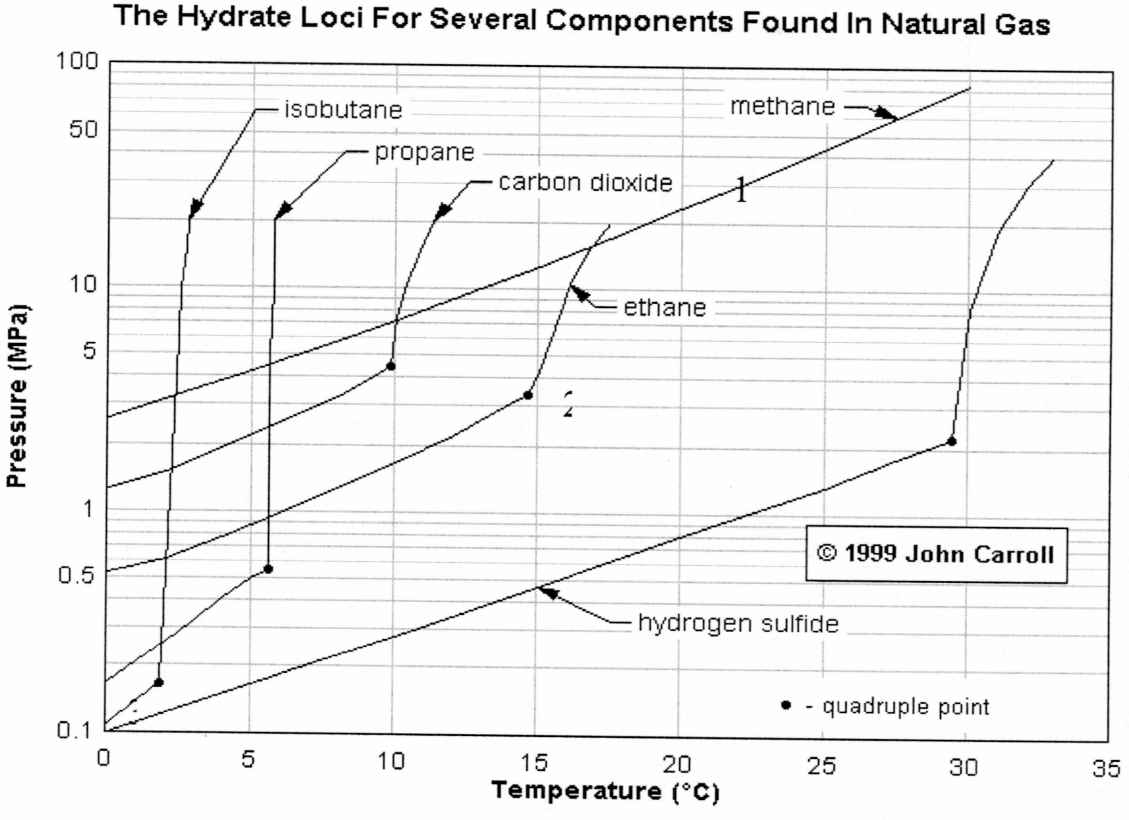

Figure 2.5: Hydrate Thermodynamics

1) Equilibrium between hydrocarbon gas, liquid water, and hydrate
2) (Upper) Equilibrium between hydrocarbon gas, liquid water, and hydrate
3) (Lower) Equilibrium between hydrocarbon gas, ice, water, and hydrate

2.6 Hydrate Stability Zones in the Alaskan Arctic

Many variables are associated with the formation of gas hydrates in the Alaskan arctic. The essential condition for hydrate formation is that the actual earth temperature is lower than the hydrate stability equilibrium temperature at a given depth.

Cold surface temperatures in polar regions promote the occurrence of permafrost, and the resulting cold temperatures at depths in the permafrost regions lead to conditions appropriate for gas hydrate deposit stability (Kvenvolden, 1998). Permafrost is perennial frozen ground for two or more consecutive years. Typical variables that effect the formation of hydrates include gas composition, depth of permafrost, salinity, geothermal gradients, pressure gradients, and the porous media properties in which hydrates form. All the variables mentioned above can, and do vary with different locations on the North Slope of Alaska.

Except for the gas composition, these variables allow the pressure/temperature conditions in the earth to be determined. Together with gas compositions, pressures and temperatures determine whether hydrates are stable (Holder et al., 1987). Collett (1993) has developed two simple equations that predicted the methane hydrate stability curve. These curves are based on the work done by Holder and Hand in 1982. One curve is

below the freezing point of water (Equation 3) while the other is above (Equation 4). The two equations are given below. Throughout the past decade many investigators have developed equations that predict the equilibrium temperatures and pressures for the methane hydrate stability curves. No one equation has been proven to be more accurate than another.

$$P = \exp\left[14.7170 - \frac{1886.79}{T}\right] \qquad \text{for } 248 \le T \le 273 \qquad (3)$$

$$P = \exp\left[38.9803 - \frac{8533.80}{T}\right] \qquad \text{for } 273 \le T \le 298 \qquad (4)$$

$P = \text{Pressure } [kPa]$

$T = \text{Temperature } [K]$

2.6.1 Pressure Gradients

Osterkamp and Payne (1981) have suggested that subsurface pressure on the North Slope of Alaska can be assumed to be in hydrostatic equilibrium. The hydrostatic pressure gradient is approximately 0.433 psia/ft. Sensitivity analysis conducted on the pressure gradient by Godbole and others (1988) shows that the hydrate stability zone increases by about 2.75% with an increase in pressure gradient above the hydrostatic equilibrium value.

2.6.2 Geothermal Gradient

Significant research efforts have been dedicated towards the effect of geothermal gradients in the North Slope of Alaska. Lachenbruch and others (1988) studied temperature profiles in ten wells located in the Kuparuk, Milne Point, and Prudhoe Bay oil fields. Using borehole temperatures they showed that isotherms converge to the west indicating an increasing thermal gradient both within and below permafrost. This increasing thermal gradient results in a westward thinning of both the permafrost and the hydrate stability zone. Since the geothermal gradient changes laterally in the North Slope region, an average regional gradient cannot be used to calculate the thickness of the zone of potential hydrate occurrence at every location.

Values in the ice-bering permafrost sequence range from approximately 1.5 °C/100 m in the Prudhoe Bay area to approximately 4.5 °C/100 m in the east-central NPRA. Geothermal gradients below the ice-bering permafrost sequence range from approximately 1.6 °C/100 m to approximately 5.2 °C/100 m (Collett, 1993). Studies done by Holder and others (1987) concluded that as the permafrost thickness increases, so does the hydrate stability zone.

Local variations in the geothermal gradients can be attributed to three main factors: 1) local effects of bodies of water on temperature at the solid earth surface, 2) lateral variations in heat flow from below permafrost, and 2) lateral variations in thermal conductivity of the permafrost (Marshall et al., 1987).

The mean surface temperature on the North Slope is approximately -11° C. About 30-50 percent of the surface is covered by lakes. Lakes deeper than about six feet will not freeze to the bottom, and consequently they have a mean bottom temperature slightly above freezing. This can cause a difference between the mean surface temperature of approximately 10° C, which will ultimately affect the geothermal gradient (Marshall et al., 1987).

The geothermal gradient within permafrost is a function of the mean thermal conductivity of the permafrost and the rate at which heat enters the base of the permafrost. Any local variations in either of these variables can cause the gradient to change. Equation 5 is a simple expression that shows this relationship.

$$\Gamma^* = \frac{q}{w} \qquad (5)$$

Γ^* = Geothermal Gradient

q = Rate at which heat enters the base of the Permafrost

w = (harmonic) mean thermal conductivity

2.6.3 Gas Composition

The composition of the gas that forms hydrates is another variable that has to be highly considered when determining the thickness of the hydrate stability zones. The presence of small quantities of heavier hydrocarbons such as propane, iso-butane, and n-butane significantly alter the hydrate equilibrium conditions (Kamath et al., 1987). For example, a 50% decrease in pressure is needed to form structure II hydrates when as little as 1% propane is added to methane (Sloan, 2000). Holder and others (1987) noted that natural gases containing propane and H_2S have the greatest effect on the hydrate stability curve compared with pure methane. In Holder's and others studies (1987) the effect of composition on the depth of the hydrate stability zone can vary from 300 feet to 600 feet. They also conclude that the composition is a more important variable beneath the permafrost because temperatures are higher beneath the permafrost and the hydrate equilibrium pressure changes to a greater extent with composition at higher temperatures.

Collett (1993) analyzed mud-log gas-chromatographic data from 320 wells and indicated that methane is the dominant hydrocarbon gas in the near-surface (0-1500 m) sedimentary rocks of the North Slope. Valin and Collett (1992) performed molecular analysis on gas sample from 10 production wells in the Prudhoe Bay, Kuparuk River, and Milne Point Units on the North Slope of Alaska and found that methane is the primary hydrocarbon gas in the gas hydrate-bearing stratigraphic units. They also concluded through isotropic analysis that both

microbial and thermogenic processes have contributed to the formation of this methane. Approximately 50 to 70 percent of the methane is thermogenic in origin and has migrated from the deeper reservoirs in the area.

Geochemical analysis on a core sample recovered from the Northwest Eileen Well No. 2 in 1972 revealed that methane is the dominant gas. The drill-stem test showed that approximately 93% is methane while the other 7% consisted of Nitrogen (Nitrogen may have been a non-native gas associated with well completion). The pressure-core barrel test showed that methane ranged from 87% to 99% methane (Collett, 1993).

2.6.4 Effects of Porous Media on Hydrates

The actual thickness of the hydrate stability zones can be greatly overestimated by neglecting the effect of the pores, that is, by assuming bulk phase behavior (Klauda and Sandler, 2001). The formation of gas hydrates in a porous media should be described by the van der Waals and Platteeuw equation for bulk hydrates with the addition of a capillary pressure term (Zhang et al., 2002). Zhang and Smith (2003) have developed a thermodynamic equation that relates the equilibrium pressure to the equilibrium temperature for gas hydrates in limited spaces (Equation 6). This equation is valid for the hydrate-liquid water equilibrium in each of the different pore sizes.

$$-\sum_i v_i \ln(1-\sum_k y_{ki})\Big|_{pore} =$$

$$\frac{\Delta\mu_w^0}{RT_0} - \int_{T_0}^{T_f} \frac{\Delta h_w^{liq}}{RT^2} dT + \int_{P_0}^{P_l = P_g - \frac{2\sigma_{H-w}}{r}\cos\theta} \frac{\Delta v_w^{liq}}{RT_f} dP - \ln(\gamma_w X_w) + \frac{2\sigma_{H-w} V_l}{rRT_f}\cos\theta$$

$$(T_f \geq T_q) \qquad (6)$$

$\Delta\mu_w$ Difference in chemical potential between empty hydrate cage and aqueous phase in equilibrium with hydrate, and $\Delta\mu_w^0$, the one at standard state.

Δv_w^{liq} Difference in mole volume between empty hydrate and the liquid.

Δh_w^{liq} Difference in enthalpies between empty hydrate and the liquid.

v_i Number of type *i* cavities per water molecule.

V_l Mole volume of water.

γ_w Activity coefficient of liquid water.

X_w Molar fraction of water.

σ_{H-w} Surface tension of hydrate-water interface.

θ Porous host-water contact angle.

r Pore radii.

R Gas Constant

y_{ki} The fractional occupation of cavity type i and Langmuir constants of the cavity i for gas k.

T_f Temperature at formation.

T_0 Temperature at standard conditions.

T_q Temperature at quadruple point.

P_l Pressure on liquid phase.

P_g Pressure on gas phase

When analyzing hydrate formation in porous media, it is important to have sufficient contact between the two phases. The interfacial tension is one of the major factors that control the contact between the phases. Yousif and Sloan (1991) investigated the effects of interfacial tension on the formation of gas hydrates in a Berea sandstone. They developed a simple equation (Equation 7) that would estimated the additional pressure required to form hydrates in a porous media at a given temperature (Yousif and Sloan, 1991).

$$\Delta p = 3.26399\sigma\left(\frac{\phi}{k}\right)^{\frac{1}{2}} \tag{7}$$

Δp Change in pressure (psia)

σ Interfacial tension (dynes/cm)

k Permeability (md)

ϕ Porosity (fraction)

The amount of gas that can be produced from a gas hydrate reservoir depends partly on the porosity. The porosity for gas hydrate bearing shallow sand reservoirs on the North Slope of Alaska ranges from 37 to 42 percent with up to an 85 percent gas hydrate saturation (Collett et al., 1988). Smosna and Mroz (1988) analyzed sandstone from the National Petroleum Reserve in Alaska and found that there are three major geologic controls that affect the porosity: 1) clay content, 2) abundance of ductile minerals, and 3) burial history. Smosna and Mroz also stated that production of gas from gas hydrates by thermal expansion may not be successful if the porosities are less then 15 percent. This constraint could seriously limit production potential of many offshore gas hydrate accumulations.

The formation of hydrates in porous media usually occurs as individual hydrate grains found in the pores of sedimentary rocks. Microscopic studies have shown that gas hydrates accumulate as films on particle surfaces, conglomerates of thin micro crystals, and separate porphyries, entirely filling the pores. On a larger scale gas hydrates can have two macro-structures: porous, resembling snow and semi- transparent, massive inclusions resembling ice (Chuvilin and Yakushev, 1998). In most cases, gas hydrates can range from a few centimeters

to tens of meters within the matrix of the porous media. This is not always the case, massive hydrates layers have occurred as thick as four meters.

2.6.5 Effects of Salinity

Collett (1993) analyzed 55 water samples taken during petroleum formation testing below the permafrost on the North Slope of Alaska. His results indicate that pore-water salinities range from 0.5 to 19 parts per thousand. With a maximum salinity of 19 ppt, the hydrate stability curve would only shift by -1.0 °C. Salinities found in the permafrost region range from 5 to 14 ppt (Osterkamp and Payne, 1981). In any case, the presence of salt in the formation fluid will ultimately depress the hydrate stability zone to some degree.

CHAPTER THREE

EXPERIMENTAL PROCESS

3.1 Hydrate Formation in a Laboratory

Methane hydrates are mainly found in hostile environments which make it very difficult to extract and test samples while trying to maintain reservoir conditions. To overcome this obstacle gas hydrates are commonly synthetically formed in laboratories where the temperature and pressure conditions can be closely monitored. Figure 3.1 shows one such testing apparatus.

Gas hydrates can be formed in a laboratory by at least three different methods. Gas can be introduced into a specimen that initially contains: seed ice, water-saturated sediment, or partially water-saturated sediment. Each of these methods will produce results that simulate natural conditions to some degree (Winters et al., 2002). In this study, fully water-saturated sediment was analyzed.

3.2 Description of Experimental Apparatus

The experimental apparatus used in this study was supplied by Oilphase-DBR, a subsidiary of Schlumberger. The apparatus consisted of an airbath that allowed the temperature to be regulated, a motorized pump that controlled the pressure, a sapphire cell in which hydrates can be formed without the presence of a porous media, a porous media cell, and a data acquisition system that controlled the system and allowed data to be recorded. Figure 3.1 shows the actual testing apparatus in which the experiments were

performed. To fully understand how the apparatus works a schematic can be seen in Figure 3.2. The airbath has the capabilities to regulate temperatures from -94 to 392 °F while the motorized pump can control pressures ranging from 0 to 3000 psia.

Conosol 260, distributed by Penreco is the hydraulic fluid used to pressurize the pump. Due to the fluid properties of Conosol 260, experiments could only be conducted between -40 and 200 °F, which was sufficient for this study. The data acquisition system recorded the following; pressure inside the cell, temperature inside the cell, temperature of the airbath, pump pressure, and pump displacement used to maintain pressure.

Figure 3.1: Hydrate Experimental Apparatus

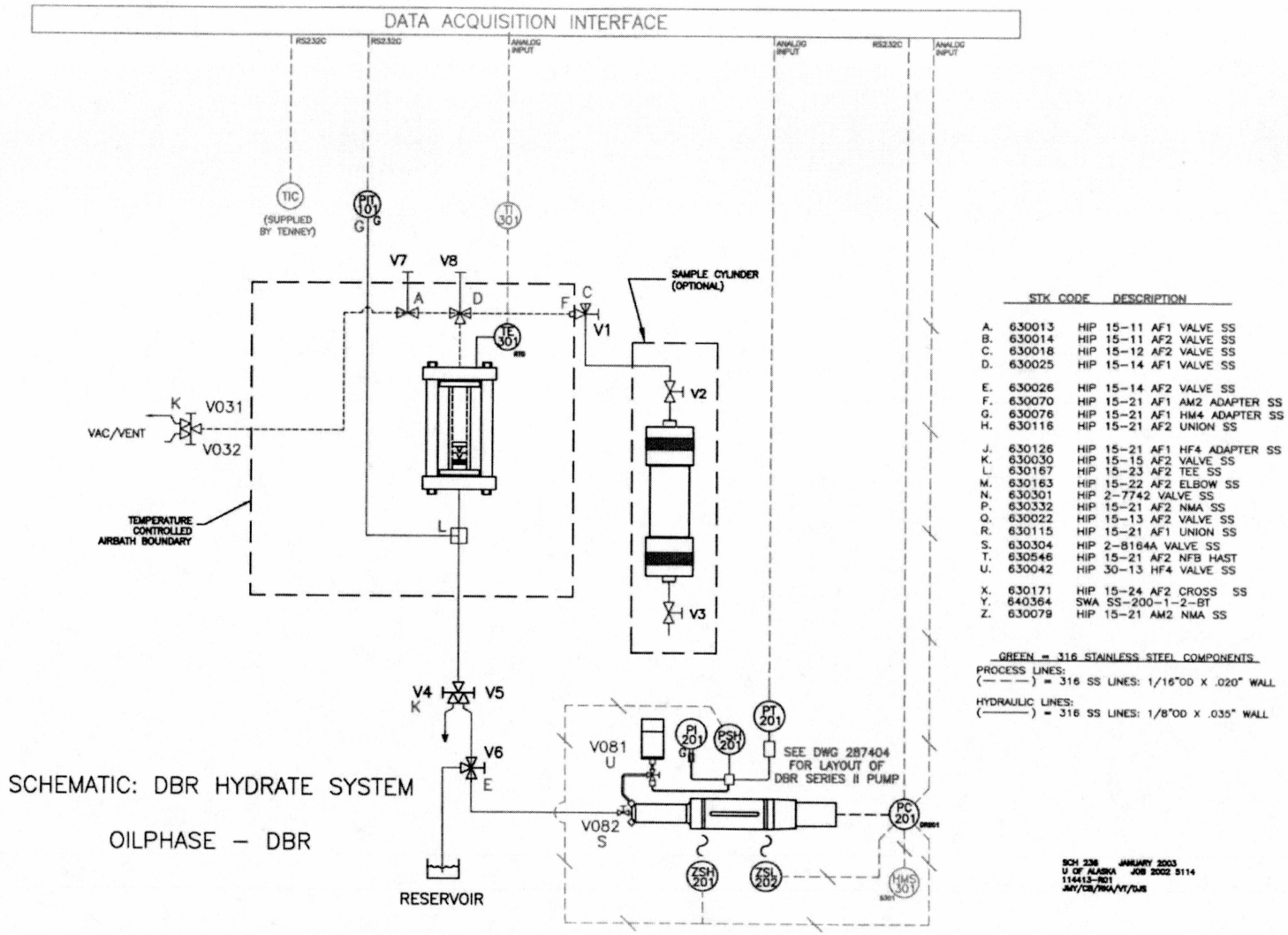

Figure 3.2: Schematic of Testing Apparatus

3.3 Procedure for Hydrates without a Porous Media

1. All air in the system was vacuumed out using a vacuum pump to ensure no air would be present during the experiments. The sapphire cell (Figure 3.4) was then injected with a 2% NaCl brine by weight through valve 31 as shown on the schematic (Figure 3.2). The methane, which was cp grade (99% Pure) was injected also though valve 31. The brine was made using distilled water and sodium chloride that was supplied by Sigma-Aldrich (99+% pure).
2. Using equilibrium temperatures and pressures predicted by the software HYDRATE 5.1 (Table 3.1 and 3.2), supplied by DBR-Oilphase, temperatures were set 5° to 10° F below the equilibrium temperatures for a given pressure. During hydrate formation a mixer mixed the fluids to ensure the methane was well mixed with the water.
3. Visual observations were made until hydrates formed. Once the hydrates were formed, the airbath temperature was gradually increased. At this point a digital camera with high resolution was placed in front of the airbath and zoomed in on a single hydrate droplet. Photos were taken anywhere from a minute to five minute increments for 12 to 24 hours. Figure 3.3 shows photos of gas hydrates dissociating at a pressure of 1500 psia. In this experiment, 99% pure methane and a 2% brine solution were used. The digital photos for all the experiments are presented in the appendix.

99% Methane, 1% Ethane, and 2.0% Brine				
Pressure (psia)	Temp (°F)	Freezing Temp (°F)	Structure	Calculation Type
3000	66.92	30.03	Struc I	Aqueous Phase
2000	61.35	30.03	Struc I	Aqueous Phase
1500	57.12	30.03	Struc I	Aqueous Phase
1200	53.63	30.03	Struc I	Aqueous Phase
900	48.9	30.03	Struc I	Aqueous Phase
600	41.85	30.03	Struc I	Aqueous Phase
300	29.27	30.03	Struc I	Aqueous Phase
100	8.66	30.03	Struc I	Aqueous Phase

Table 3.1: Software Predictions for a 2% by Weight Brine Solution

99% Methane, 1% Ethane, and 4.0% Brine				
Pressure (psia)	Temp (°F)	Freezing Temp (°F)	Structure	Calculation Type
3000	65.51	27.88	Struc I	Aqueous Phase
2000	59.98	27.88	Struc I	Aqueous Phase
1500	55.77	27.88	Struc I	Aqueous Phase
1200	52.3	27.88	Struc I	Aqueous Phase
900	47.59	27.88	Struc I	Aqueous Phase
600	40.56	27.88	Struc I	Aqueous Phase
300	27.9	27.88	Struc I	Aqueous Phase
100	7.44	27.88	Struc I	Aqueous Phase

Table 3.2: Software Predictions for a 4% by Weight Brine Solution

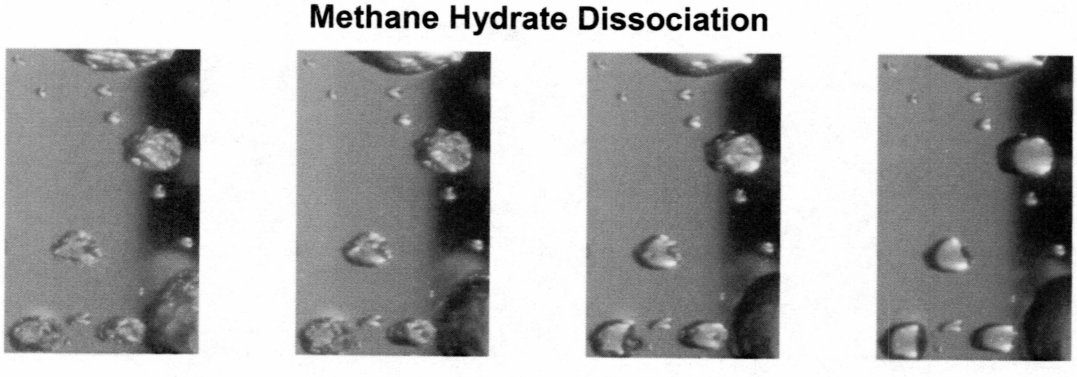

Figure 3.3: Visual Observations of Hydrate Dissociation in 2% Brine at 1500 psia

4. The digital photos were then viewed in a movie format to determine where the hydrates started "melting" (dissociating). The time on the photo that showed the hydrates dissociating was then compared to the time on the data acquisition system to determine the sapphire cell temperature and pressure for hydrate dissociation. Both the camera's time and the data acquisition's time were synchronized to the same time.
5. Experiments were conducted for pressures of 1500, 1200, 900, 600, and 300 psia.
6. This process was repeated for an additional NaCl concentration of 4% by weight.
7. The temperatures and pressures were then used along with the geothermal gradient to determine the extent of the hydrate stability zone.

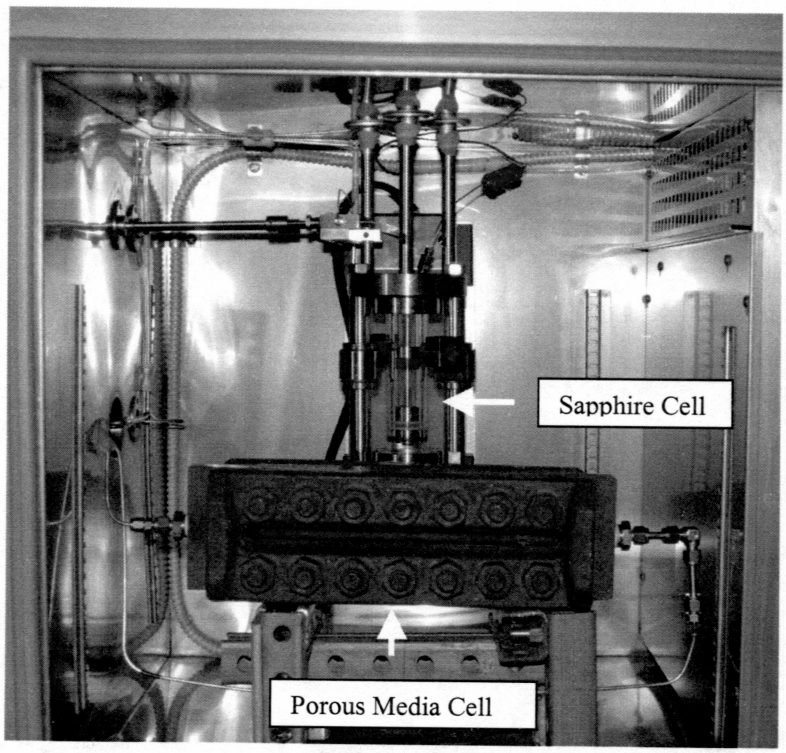

Figure 3.4: Sapphire and Porous Media Testing Cells

3.4 Procedure for Porous Media Experiments

1. Industrial quartz sand with a porosity of 60% and a permeability of 15 md was used to pack the porous media cell (Figure 3.3). The porosity and permeability were measured in a rock and fluid laboratory. A vacuum pump was connected to one end while the other end was connected to a brine reservoir (NaCl concentration of 2% by weight). The vacuum pump was then turned on and was used to fully saturate the porous media with saline solution. Steel wool was placed at both ends of the cell to ensure that no sand would be lost while prepping the cell for testing.
2. The cell was then placed in the airbath and connected to the inlet and outlet valves. Methane was then injected into the cell while the outlet valve remained open for a brief amount of time to help vacate any air that might have been trapped within the cell.
3. The methane injected into the cell passed through the sapphire cell, therefore the pressure inside the sapphire cell was the same as the pressure inside the porous media cell. This allowed the pressure inside the porous media cell to be measured. There was no thermocouple inside the porous media cell, so temperature change in the airbath was done slowly to achieve temperature equilibrium between the cell and the airbath.
4. Using the predictions calculated by the software HYDRATE 5.1, without the presence of a porous media, the cell temperature was set 5° to 10° F below the dissociation temperature at given pressure. The way the cell was designed; visual observations could not be done, so analyzing pressure changes due to the formation or

dissociation of the hydrates was done by analyzing pressure maintenance. This allowed the dissociation temperature to be determined at given pressure.

5. The temperature was maintained anywhere from 5° to 10 °F below the equilibrium temperature anywhere from 6 to 12 hours. The amount of time was dependent on analyzing the pressure change to ensure that hydrates had indeed formed.
6. With the formation of hydrates the temperature was set to raise 0.2° F every 15 minutes. This was conducted anywhere from 12 to 24 hours with data being recorded every minute.
7. As the hydrates are dissociating methane is being produced and therefore the pressure is increasing. To maintain a constant pressure the pump displacement is decreasing. The two most important variables that were recorded were the pump displacement used to maintain pressure and the time. These two variables were plotted against each other. The point in the graph where there is a major drop indicates that hydrates are starting to dissociate (Figure 3.5). At this point on the graph the corresponding time is related to the temperature and pressure recorded by the data acquisition system.
8. This process was conducted on pressures of 1500, 1200, 900, 600, and 400 psia. In conducting experiments less the 400 psia it was difficult to achieve reliable results. This may be partly due the equilibrium temperature being below the freezing point of water.
9. This process was repeated exactly the same except that a 4% NaCl concentration brine was used.

10. Steps one through nine were again repeated except in this case the porous media used was from Anadarko Hot Ice #1 well from the North Slope of Alaska. The porous media was a core that Anadarko had retrieved from a depth of 1305.5 ft. This core had a porosity that ranged anywhere from 19% to 31% and a permeability in a range of 2 to 4 md. Again these values were determined in a rock and fluid laboratory. Upon visual inspection, the core consisted of very fine particles on the order of clay or silt type sediment.
11. The temperatures and pressures were then used along with the geothermal gradient to determine the extent of the hydrate stability zone.

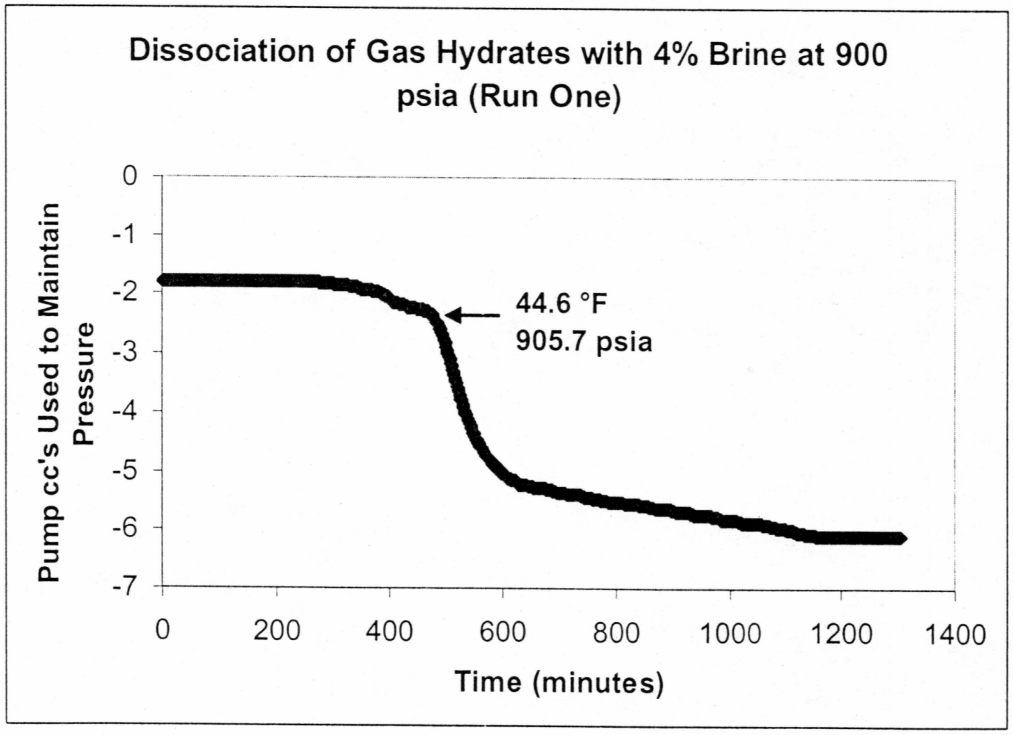

Figure 3.5: Example of Hydrate Dissociation

3.5 Procedure for Determining Hydrate Stability Zones

1. Five wells were selected from the North Slope of Alaska; West Sak River 17 (WK-17), West Sak River 14 (WK-14), West Sak River 11 (WK-11), NW Eileen State 2 (NWEN), and North Highland State #1 (NHST). Figure 3.6 shows the location of the various wells. The distance between WK-11 and NHST is approximately 19 miles. These wells were chosen because temperature log data was available in and below the permafrost which allowed the geothermal gradients to be determined.
2. Using temperature log data taken from the "USGS Borehole Temperature Log – Alaska" website, geothermal gradients in and below the permafrost were determined for WK-11, WK-14, WK-17, and NHST wells. Timothy Collett provided the geothermal gradient information for the NWEN well. In order to determine the geothermal gradients a mean annual surface temperature of -11° C was used.
3. The pressure results obtained from the experiments were converted to equivalent depth using an average pressure gradient of 0.433 psia/ft.
4. The geothermal gradient was plotted along with the dissociation temperatures and equivalent depths

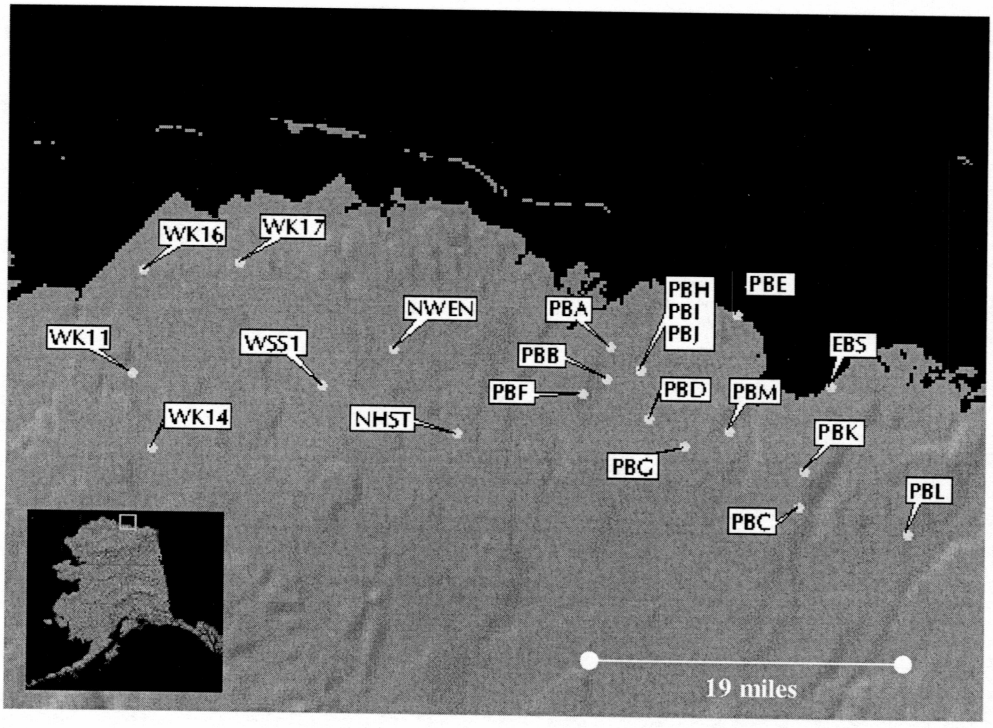

Figure 3.6: Location of Wells (USGS website)

5. The area encompassed by the two curves represents the zone for hydrate stability. The intersection at the shallowest depth is the top of the hydrate stability zone and the deeper intersection represents the bottom of the hydrate stability zone.
6. All depths were converted to meters while the temperatures were converted to Kelvin. This was done to increase the clarity of the hydrate stability zones.
7. This process was repeated for the five different wells being examined in this study

CHAPTER FOUR

RESULTS AND DISSCUSSION

4.1 Hydrate Dissociation without a Porous Media

A 2% brine and a 4% brine were used in each of the experiments. For each experiment conducted, a dissociation temperature and pressure were recorded. These values ultimately allowed the hydrate stability zone to be determined.

The sapphire cell experiments were conducted without the presence of a porous media. Hydrates were formed in the cell and then dissociated in order to determine the equilibrium pressure and temperature. The determination of the dissociation pressures and temperatures was done visually with the use of a high magnification camera. The digital photos from each of the experiments are found in Appendix A. The results obtained in these experiments are given in Table 4.1.

Using the geothermal gradients from five different wells and an average pressure gradient of 0.433 psia/ft, HSZ plots were constructed. Each curve for the five wells are shown in Figures 4.1 to 4.10

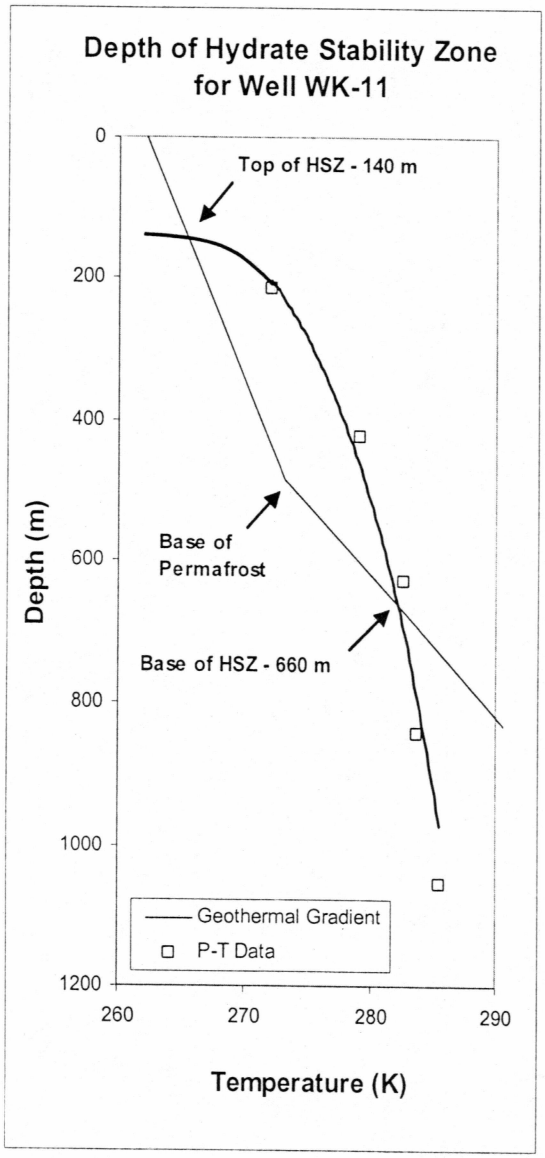

Figure 4.1: HSZ for WK-11 (2% Brine)

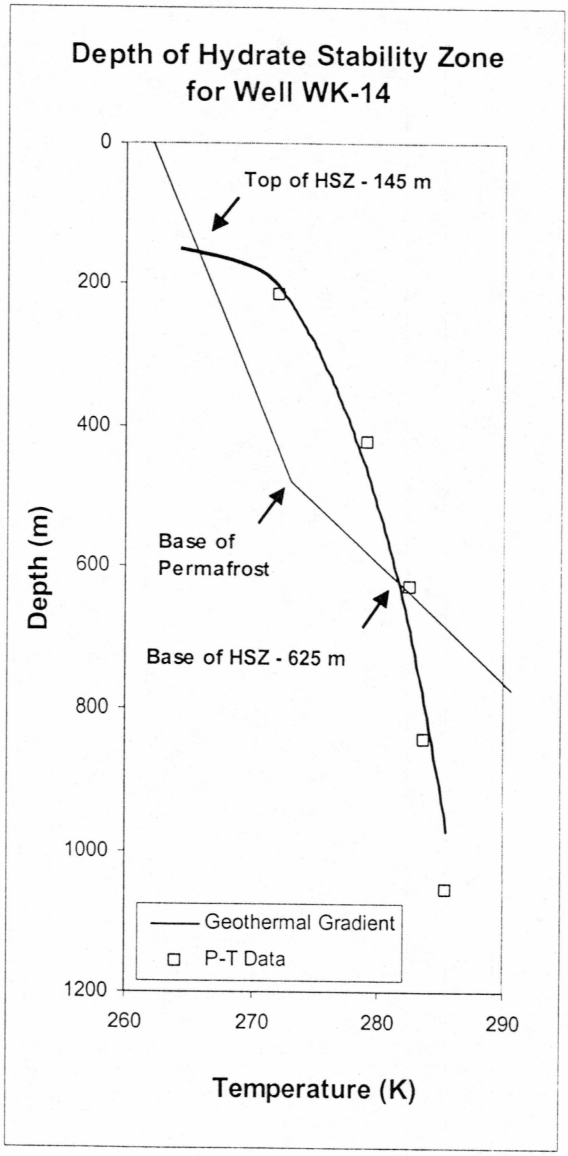

Figure 4.2: HSZ for WK-14 (2% Brine)

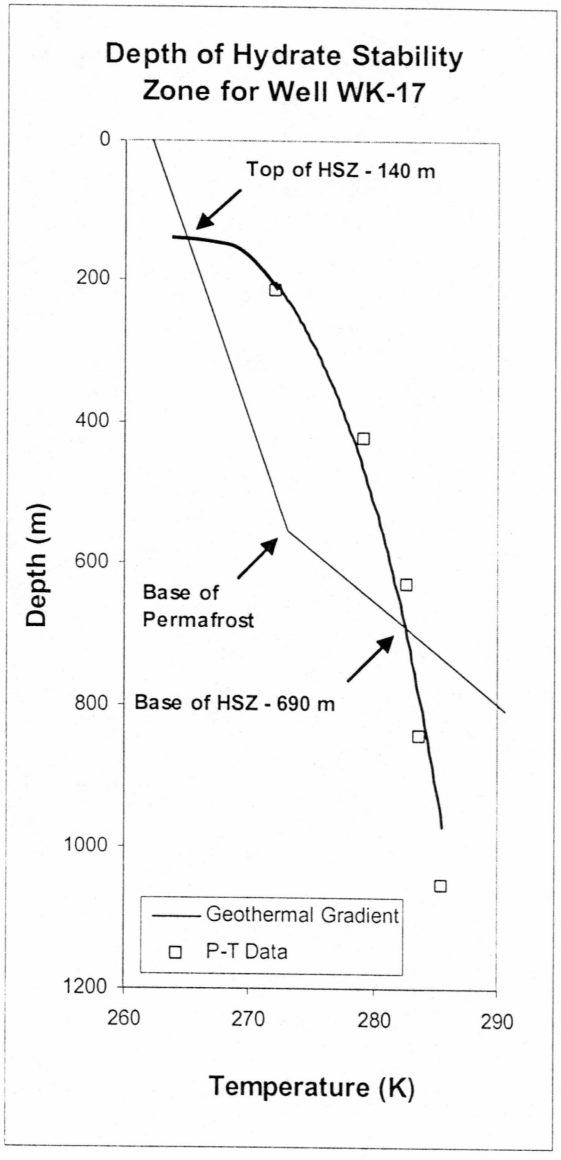

Figure 4.3: HSZ WK-17 (2% Brine)

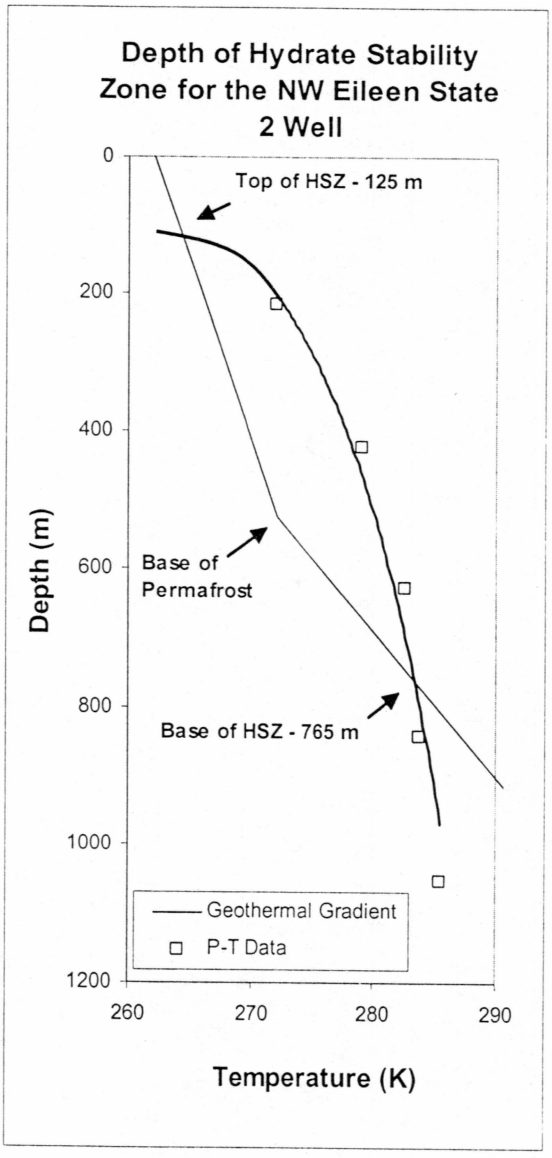

Figure 4.4: HSZ for NWEN (2% Brine)

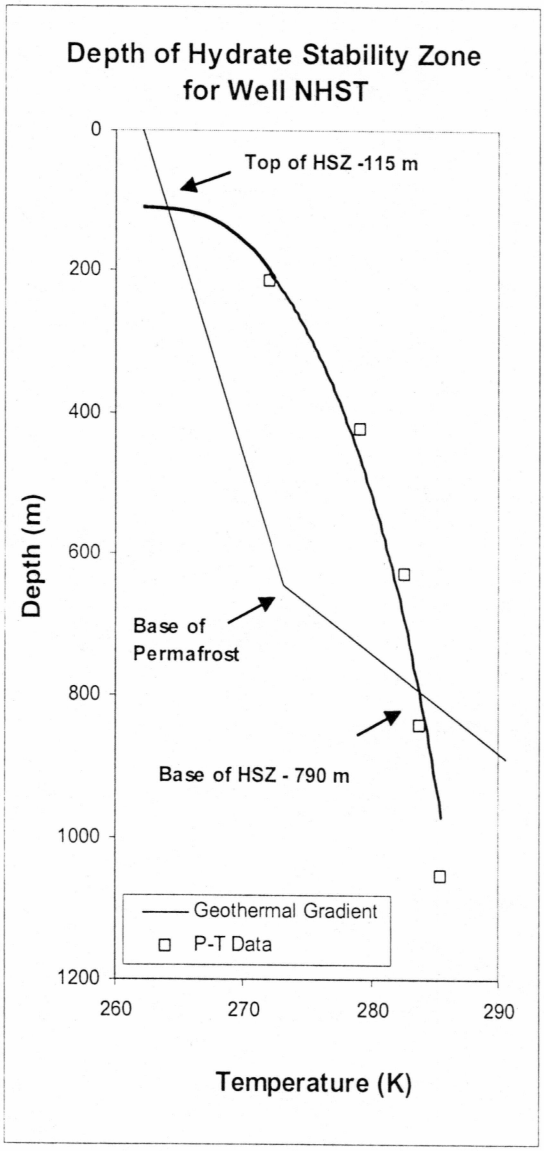

Figure 4.5: HSZ for NHST (2% Brine)

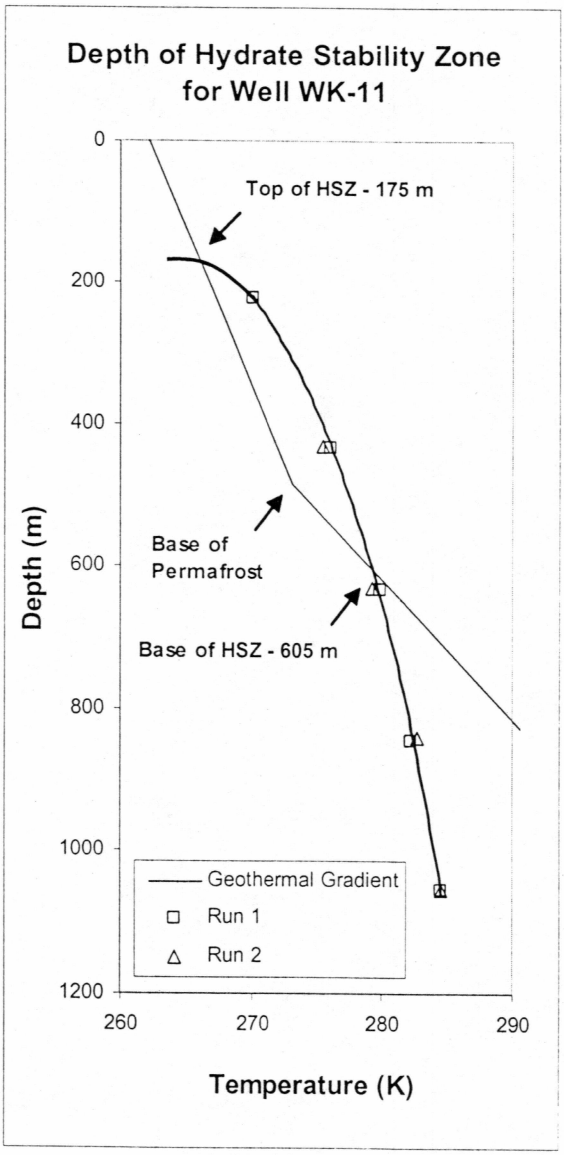

Figure 4.6: HSZ for WK-11 (4% Brine)

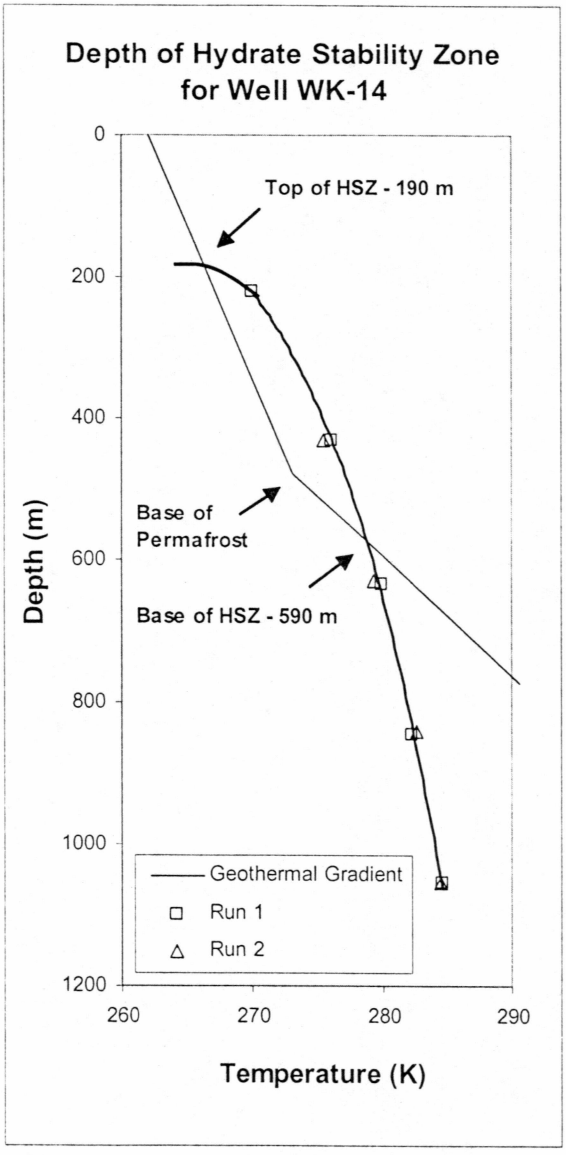

Figure 4.7: HSZ for WK-14 (4% Brine)

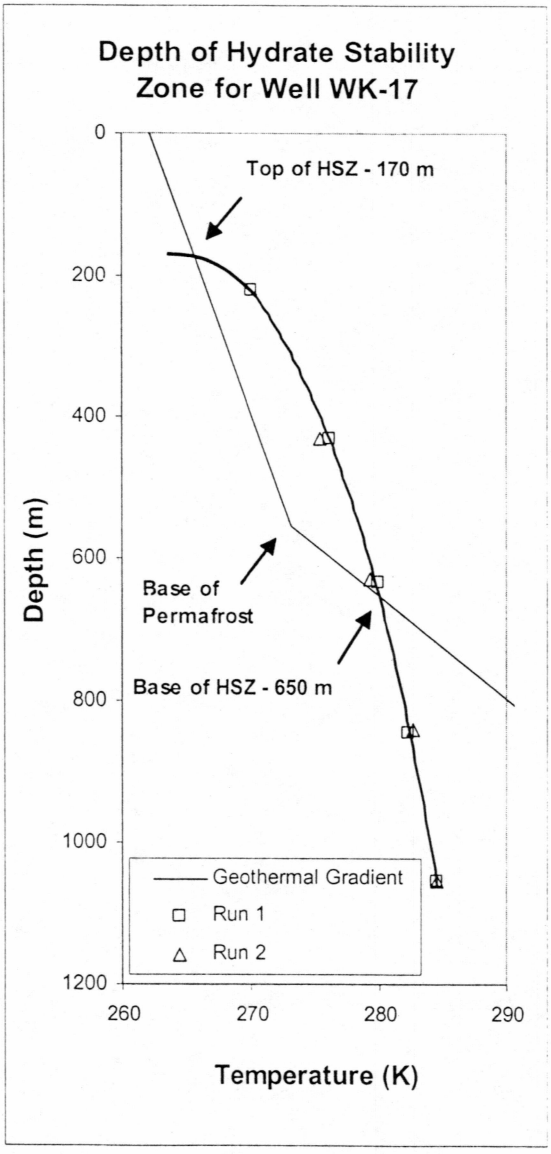

Figure 4.8: HSZ for WK-17 (4% Brine)

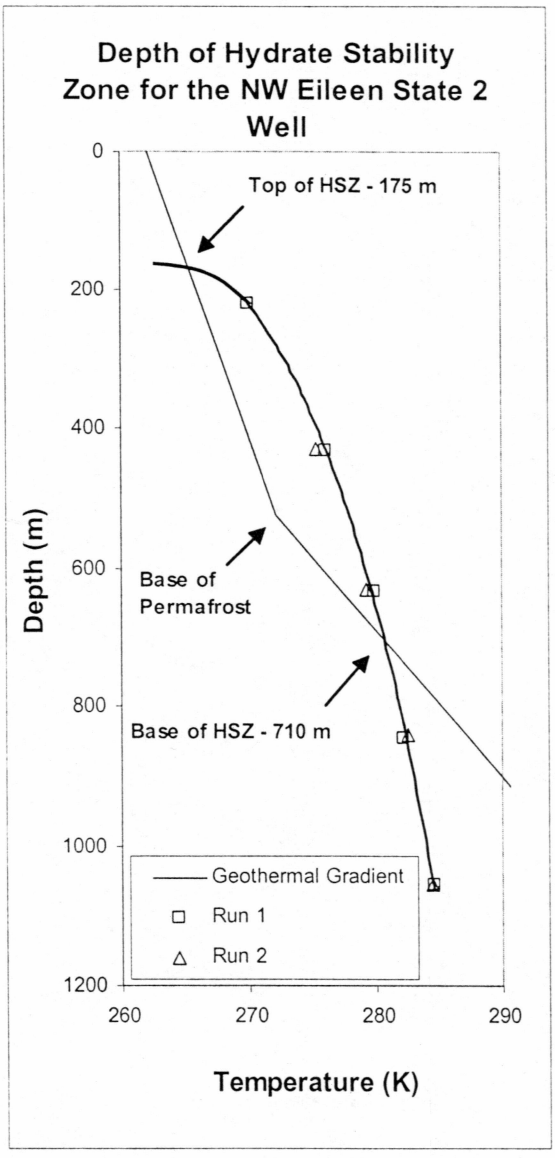

Figure 4.9: HSZ for NWEN (4% Brine)

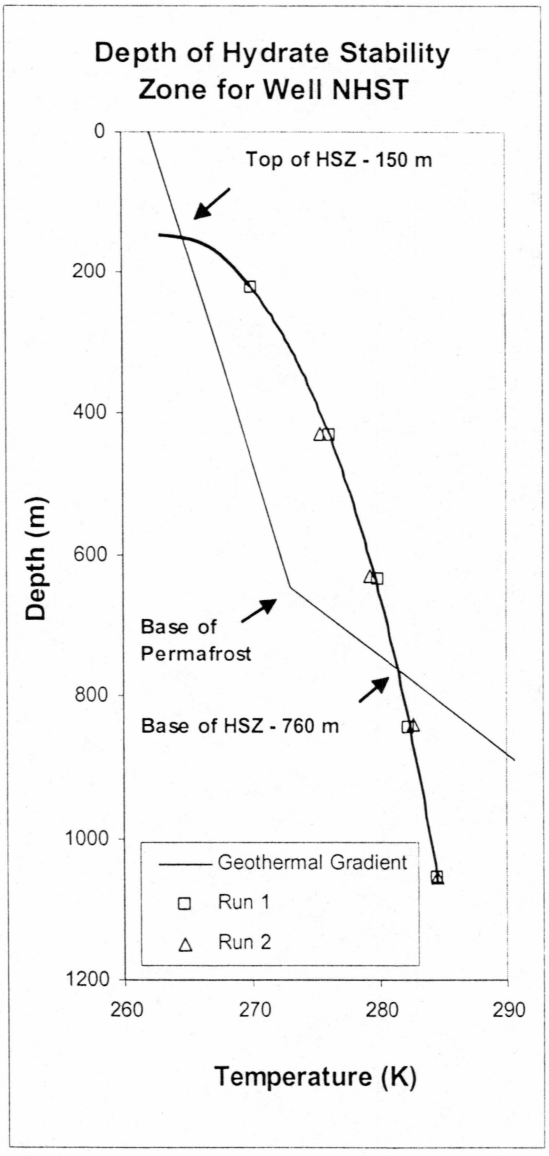

Figure 4.10: HSZ for NHST (4% Brine)

The intersections of the geothermal gradient and the hydrate stability curve determined the base and the top of the hydrate stability zone. These values are listed in Table 4.2 for both a 2% and 4% NaCl concentration by weight.

Figure 4.11 shows how the zone of hydrate stability varies between the different wells. It also shows the influence that different NaCl concentrations have on the HSZ. It is interesting to note that in both concentrations the zone of hydrate stability thickens as moving eastward and northward.

Table 4.1: Synthetic Hydrate Experimental Results

2% Brine	
Temp. (°F)	Pressure (psia)
29.9	300
42.7	600
49	892
51	1195
54.2	1497

4% Brine	
Temp. (°F)	Pressure (psia)
52.5	1499.7
52.4	1499.7
48.3	1200.7
49	1194.7
44	900.7
42.9	895.7
37.3	614.7
36	611.7
26.4	315.7

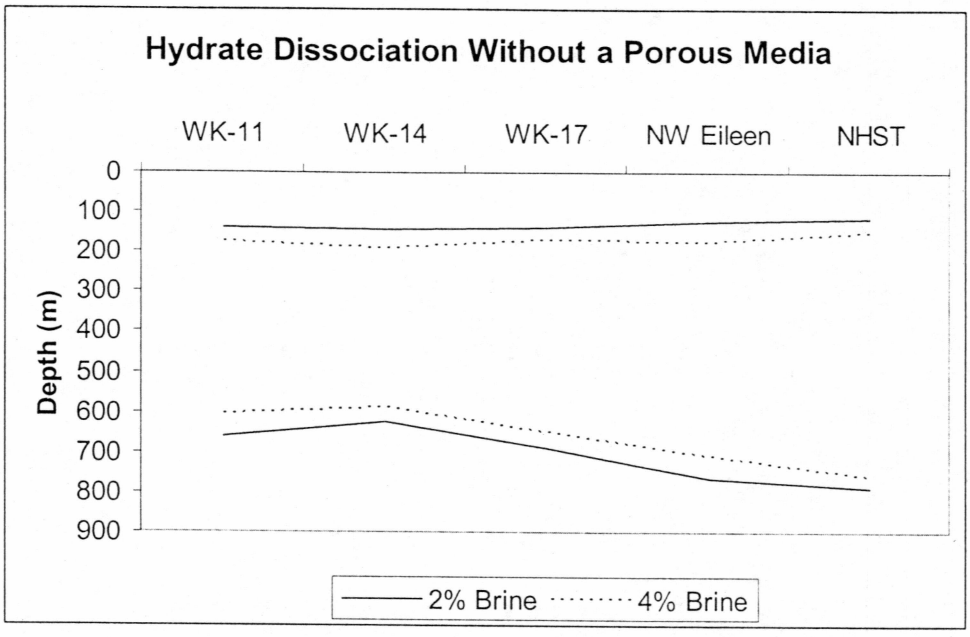

Figure 4.11: HSZ for Bulk Hydrates

Table 4.2: Extent of the Hydrate Stability Zone for Synthetic Hydrates

2% Brine			4% Brine		
Well	Top (m)	Bottom (m)	Well	Top (m)	Bottom (m)
WK-11	140	660	WK-11	175	605
WK-14	145	625	WK-14	190	590
WK-17	140	690	WK-17	170	650
NWEN	125	765	NWEN	175	710
NHST	115	790	NHST	150	760

At well WK-11 the thickness of the hydrate stability zone is approximately 520 m for a 2% brine, as for a 4% brine the thickness decreases to 430 m. Going east to well NHST, the thickness increases to 675 m with a 2% brine while the 4% brine has a thickness of 610 m. Lachenbruch and others (1987) analyzed the thickness of the HSZ from well logs for wells WK-11, WK-14, WK-17, and NHST. They determined the HSZ to be approximately 561, 568, 657, and 718 meters respectively. Their results assume zero salinity and the uncertainty ranges from ± 30-50 m. The thicknesses obtained in this study are all within approximately 100 m of Lachenbruch and others (1987) work. These results also show that a 2% brine increase, can affect the thickness of the hydrate stability zone by as much as 90 m when a porous media is not present, which coincidently is the approximate difference between Lachenbruch and others (1987) work and the results presented in this study.

4.2 Hydrate Dissociation in the Presence of a Synthetic Porous Media

The data for the porous media experiment was obtained by analyzing pressure maintenance during the hydrate dissociation. At each pressure multiple experiments were conducted to show repeatability and reproducibility. The raw data from each experiment is presented in Appendix B. The results from these experiments are given in Table 4.3.

Table 4.3: Synthetic Porous Media Experimental Results

2% Brine			4% Brine		
1500 psia			1500 psia		
	Temp. (°F)	Pressure (psia)		Temp. (°F)	Pressure (psia)
Run 1	54	1507.7	Run 1	52.2	1511.7
Run 2	55	1509.7	Run 2	51.8	1507.7
Run 3	55.2	1509.7	Run 3	52	1508.7
1200 psia			1200 psia		
	Temp. (°F)	Pressure (psia)		Temp. (°F)	Pressure (psia)
Run 1	51.7	1206.7	Run 1	47.9	1207.7
Run 2	51.3	1206.7	Run 2	48.2	1207.7
Run 3	51.4	1207.7	Run 3	48.4	1207.7
900 psia			900 psia		
	Temp. (°F)	Pressure (psia)		Temp. (°F)	Pressure (psia)
Run 1	45.2	905.7	Run 1	43.6	910.7
Run 2	45.6	904.7	Run 2	43.6	909.7
Run 3	46.1	904.7	Run 3	43.3	910.7
600 psia			600 psia		
	Temp. (°F)	Pressure (psia)		Temp. (°F)	Pressure (psia)
Run 1	38.7	601.7	Run 1	36.4	609.7
Run 2	39.8	606.7	Run 2	36.7	605.7
Run 3	38.4	602.7	Run 3	36.3	601.7
*** No data was taken at 400 psia ***			400 psia		
				Temp. (°F)	Pressure (psia)
			Run 1	31.8	401.7
			Run 2	32.7	402.7
			Run 3	N/A	N/A

These results were used to construct hydrate stability curves for the five wells (Figures 4.12 to 4.21). Again, using the geothermal gradients and an average pressure gradient of 0.433 psia/ft, the HSZ was determined (Figure 4.22).

The 2% and 4% brine experiments showed that as you move east and north the depth of the HSZ increases. These results are presented in Table 4.4. Problems arose in

achieving reliable results when conducting experiments below 400 psia. The problem is believed to do with the freezing point of water. Below this pressure the formation/dissociation temperature is below the freezing point of water. For this reason the results obtained below 400 psia were disregarded. Disregarding these results did not allow the top of the HSZ to be accurately determined. No data was taken at 400 psia for the 2% brine concentration therefore the thickness of the HSZ for the 2% brine is going to be much less then other analyses.

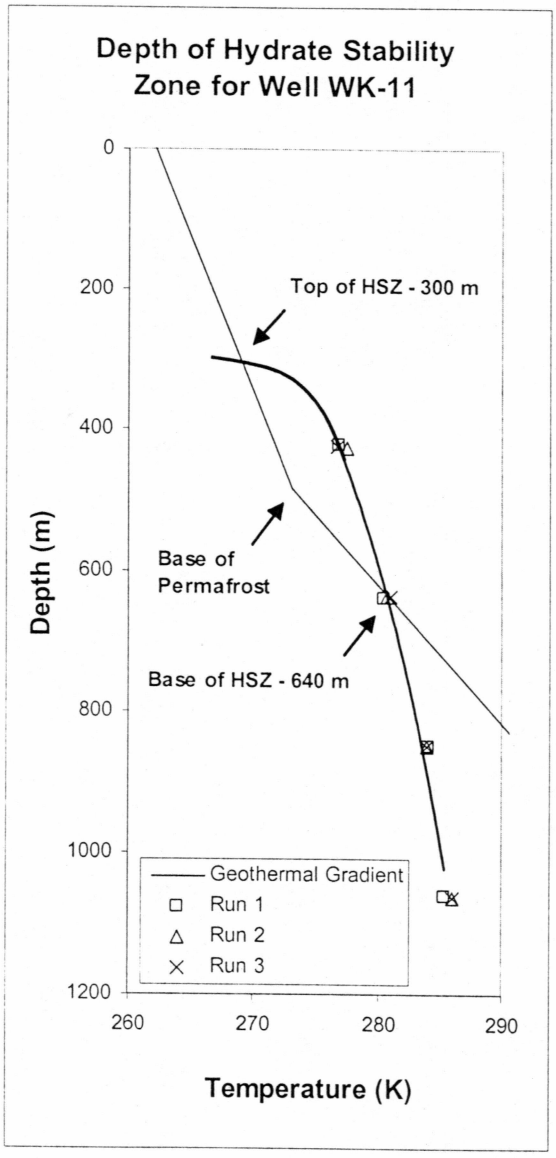

Figure 4.12: HSZ for WK-11 (2% Brine)

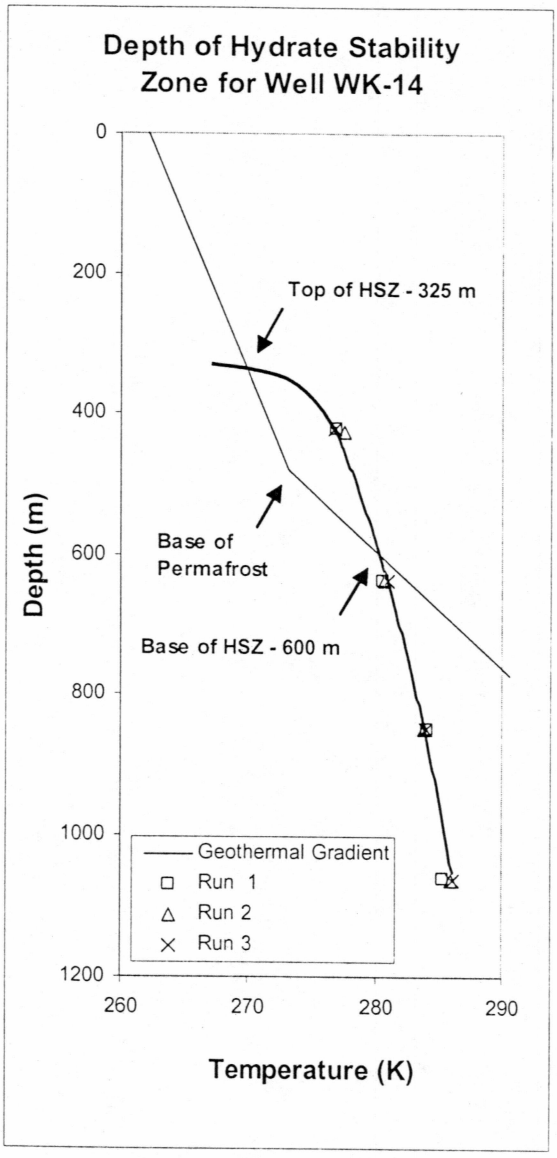

Figure 4.13: HSZ WK-14 (2% Brine)

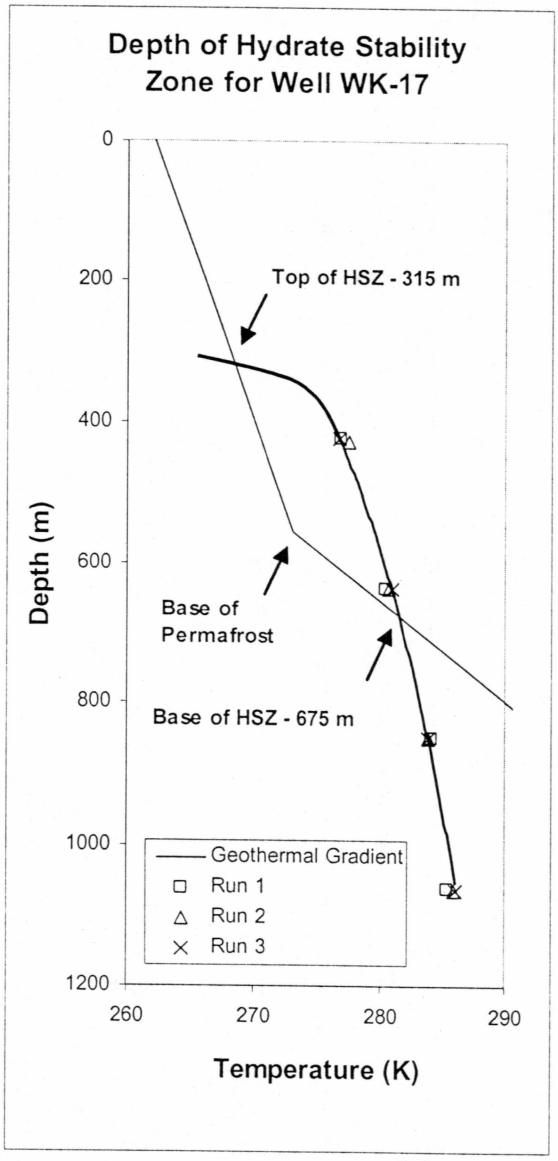

Figure 4.14: HSZ for WK-17 (2% Brine)

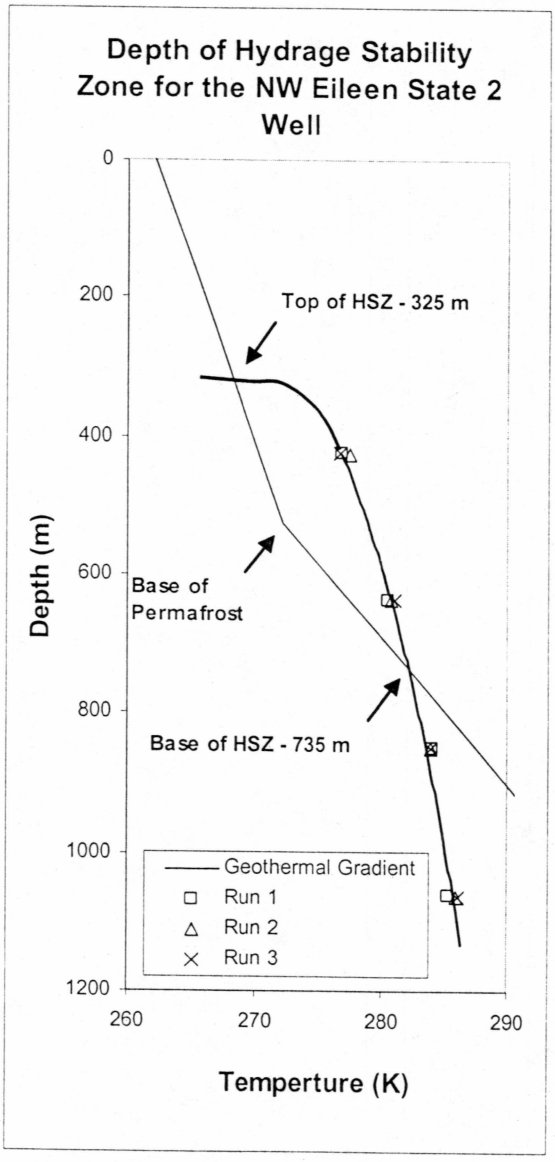

Figure 4.15: HSZ for NWEN (2% Brine)

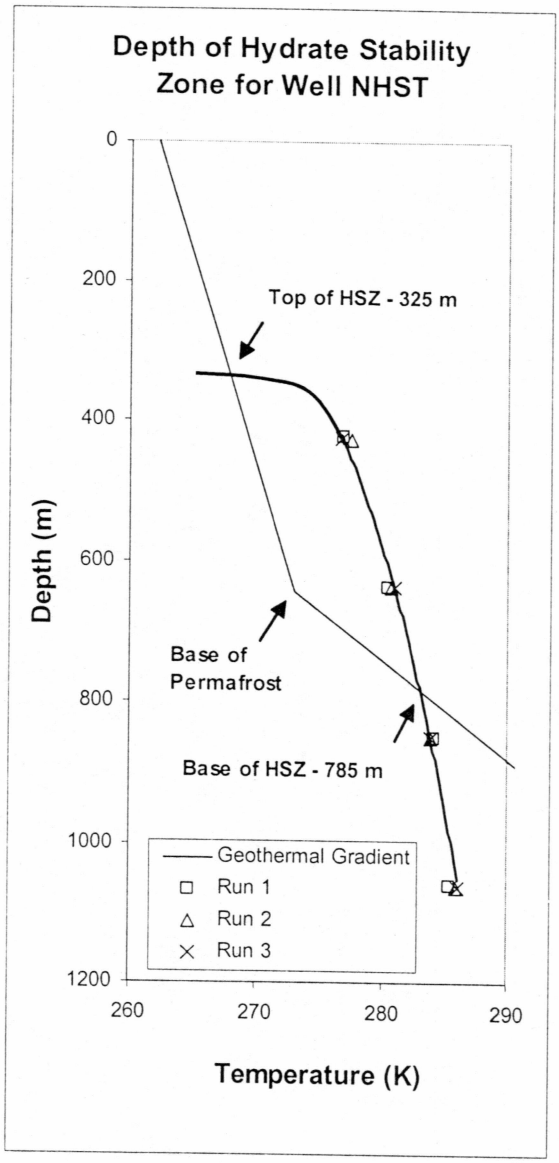

Figure 4.16: HSZ for NHST (2% Brine)

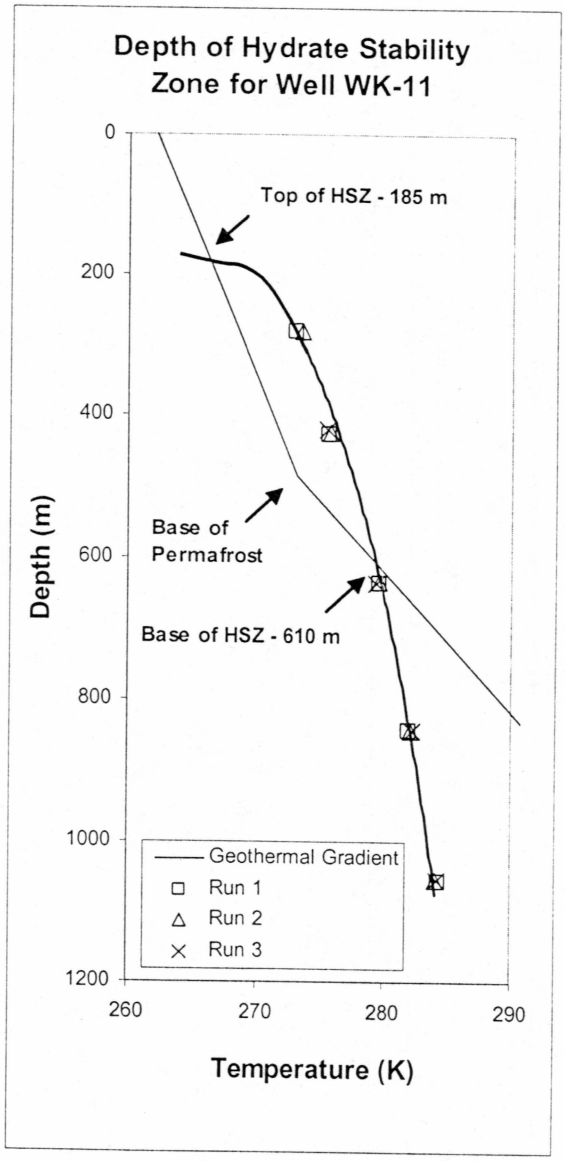

Figure 4.17: HSZ for WK-11 (4% Brine)

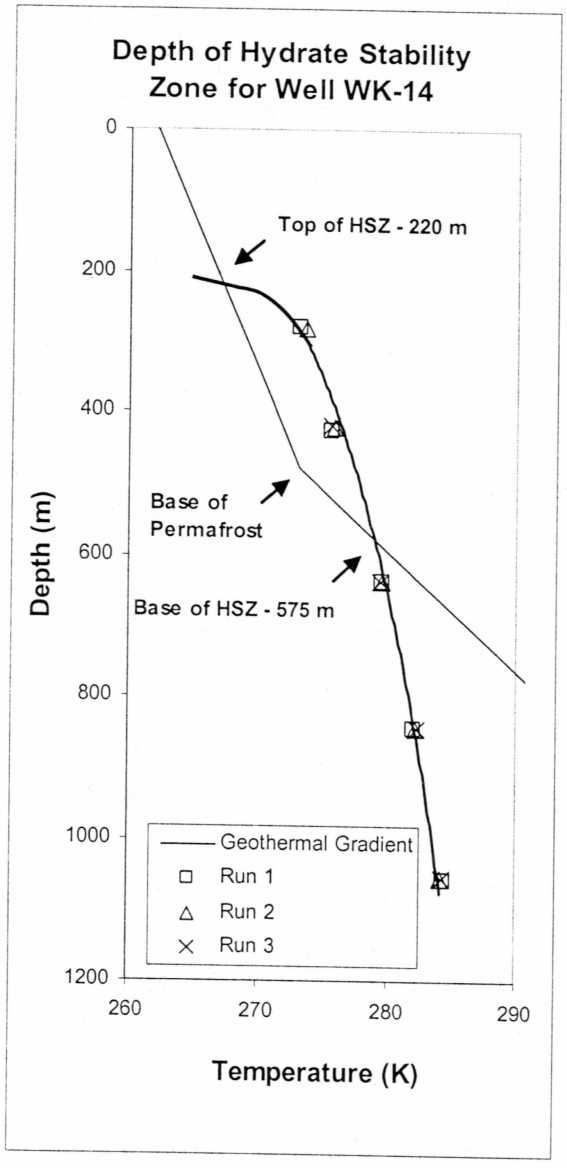

Figure 4.18: HSZ for WK-14 (4% Brine)

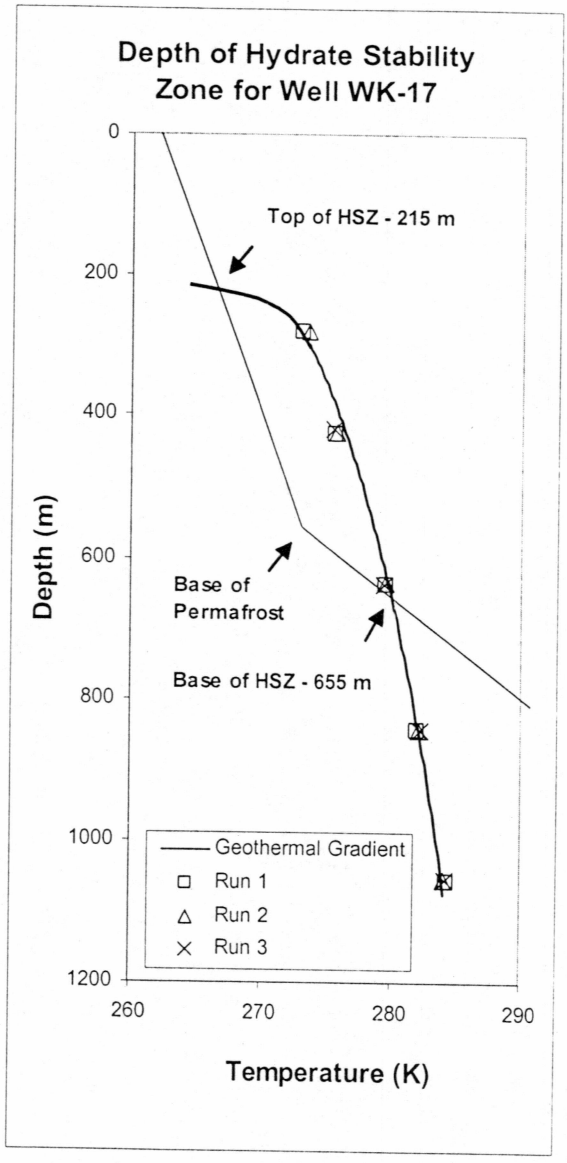

Figure 4.19: HSZ for WK-17 (4% Brine)

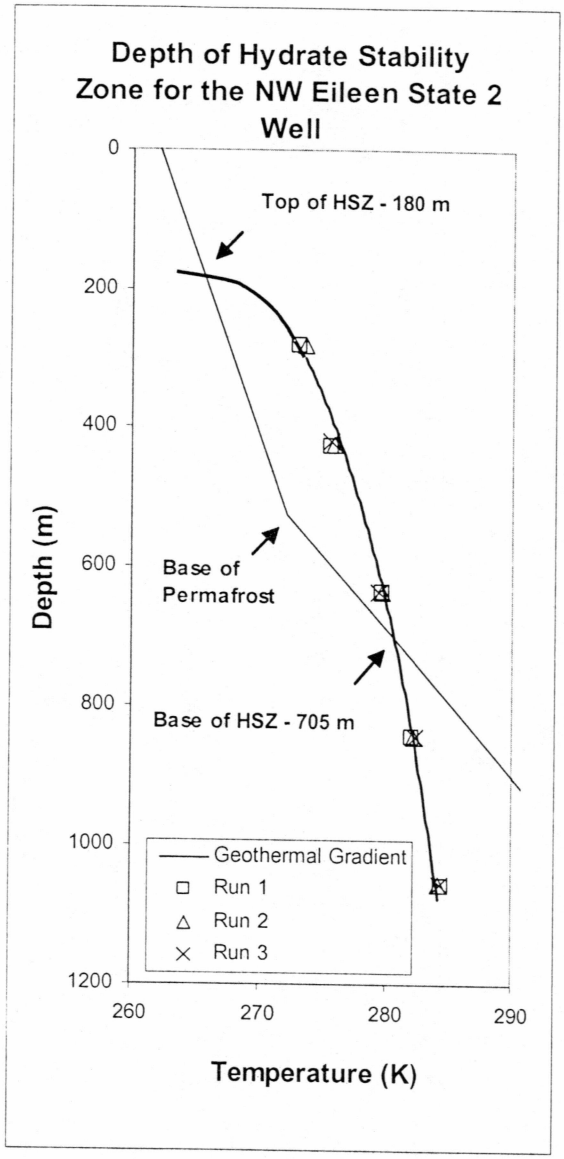

Figure 4.20: HSZ for NWEN (4% Brine)

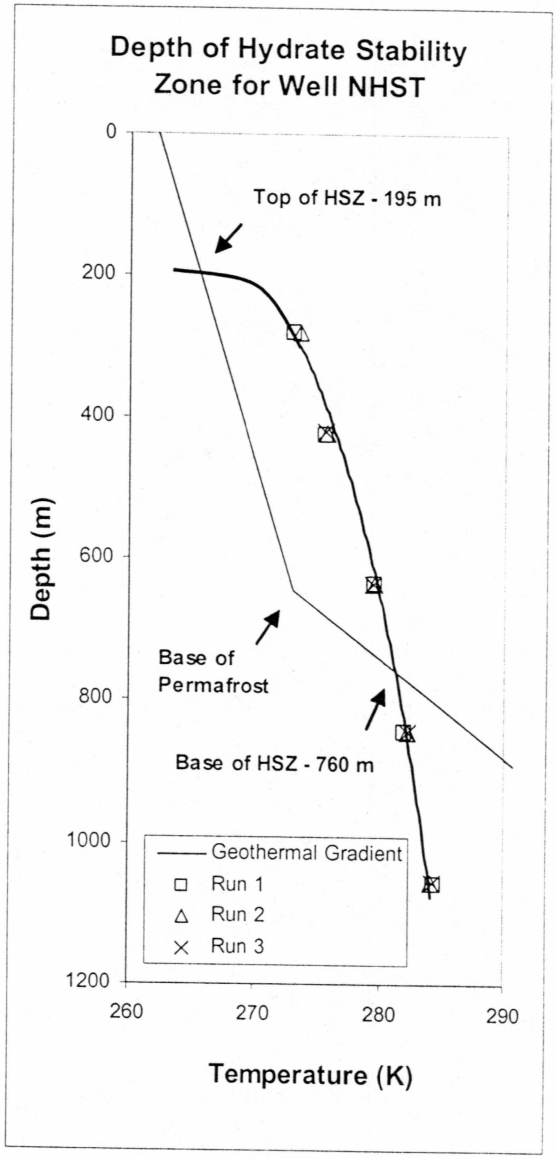

Figure 4.21: HSZ for NHST (4% Brine)

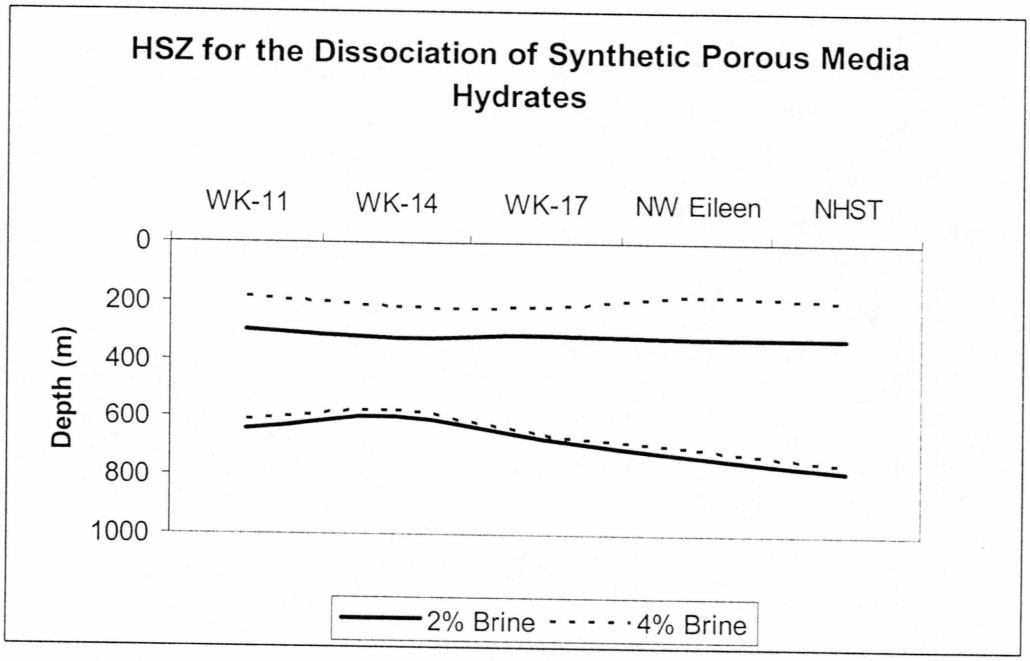

Figure 4.22: HSZ for Synthetic Porous Media Hydrates

Table 4.4: Extent of the Hydrate Stability Zone for a Synthetic Porous Media

2% Brine			4% Brine		
Well	Top (m)	Bottom (m)	Well	Top (m)	Bottom (m)
WK-11	300	640	WK-11	185	610
WK-14	325	600	WK-14	220	575
WK-17	315	675	WK-17	215	655
NWEN	325	735	NWEN	180	705
NHST	325	785	NHST	195	760

The 4% brine experiments gave thicknesses for WK-11, WK-14, WK-17, and NHST of 425, 355, 440, and 565 respectively. These values are less than the bulk hydrate experiments by 5 to 45 m. Since no data was taken at 400 psia for the 2% brine, the top of the hydrate stability zone is going to be much deeper and therefore the thickness is going to be much less than what is expected. For this reason not much analysis was given to the 2% brine experiments.

Figure 4.22 shows how the thicknesses vary as you move east for the various wells. The distance between WK-11 and NHST is approximately 19 miles. The depth of the HSZ decreases by 20 to 30 m with a brine increase of 2% when a porous media is present. Whereas the depth of the synthetic hydrate stability zone decreases by 30 to 45 m with an increase in brine concentration. This could indicate that the influence of a brine concentration on hydrate formation in the presence of a porous media only affects the depth of the HSZ by 10 to 15 m.

4.3 Hydrate Dissociation in the Presence of a Porous Media Field Sample

The field sample was supplied by the Anadarko Corporation and was taken from a depth of 1305.5 ft. This sample came from the methane hydrate research well Hot Ice #1 found on the North Slope of Alaska.

These experiments were also conducted by analyzing pressure maintenance during the hydrate dissociation. The raw data from each experiment is presented in Appendix C. The results from each of the experiments are listed in Table 4.5. From these results hydrate stability curves were constructed (Figures 4.23 to 4.32). The information

provided by these results best mimics rock properties typically found on the North Slope of Alaska.

Table 4.5: Experimental Results from Anadarko Sample

2% Brine			4% Brine		
1500 psia			1500 psia		
	Temp. (°F)	Pressure (psia)		Temp. (°F)	Pressure (psia)
Run 1	54.5	1511.7	Run 1	52.3	1505.7
Run 2	54.4	1509.7	Run 2	52.7	1505.7
Run 3	54.2	1509.7	Run 3	53.6	1508.7
1200 psia			1200 psia		
	Temp. (°F)	Pressure (psia)		Temp. (°F)	Pressure (psia)
Run 1	50.7	1206.7	Run 1	49.1	1203.7
Run 2	50.9	1210.7	Run 2	49.2	1207.7
Run 3	50.9	1209.7	Run 3	49.2	1208.7
900 psia			900 psia		
	Temp. (°F)	Pressure (psia)		Temp. (°F)	Pressure (psia)
Run 1	46.4	910.7	Run 1	44.6	905.7
Run 2	46	904.7	Run 2	44.9	908.7
Run 3	45.8	904.7	Run 3	44.8	906.7
600 psia			600 psia		
	Temp. (°F)	Pressure (psia)		Temp. (°F)	Pressure (psia)
Run 1	39.2	608.7	Run 1	37.8	604.7
Run 2	39.3	607.7	Run 2	37.8	601.7
Run 3	39.4	608.7	Run 3	37.9	603.7
400 psia			400 psia		
	Temp. (°F)	Pressure (psia)		Temp. (°F)	Pressure (psia)
Run 1	31.5	403.7	Run 1	30.7	401.7
Run 2	32.3	405.7	Run 2	30.5	398.7
Run 3	32.2	401.7	Run 3	30.5	397.7

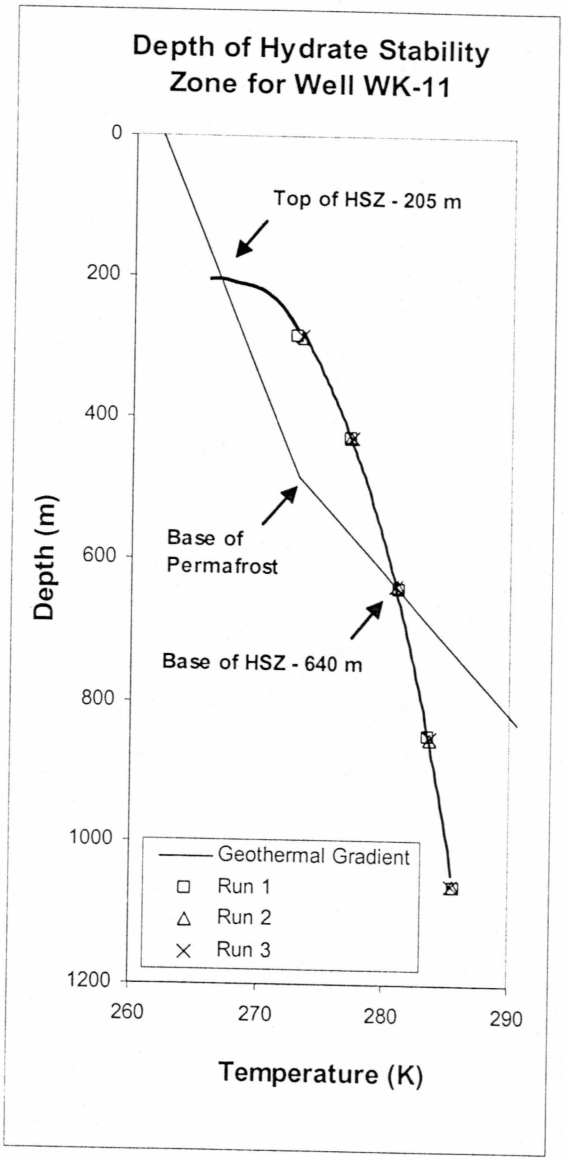

Figure 4.23: HSZ for WK-11 (2% Brine)

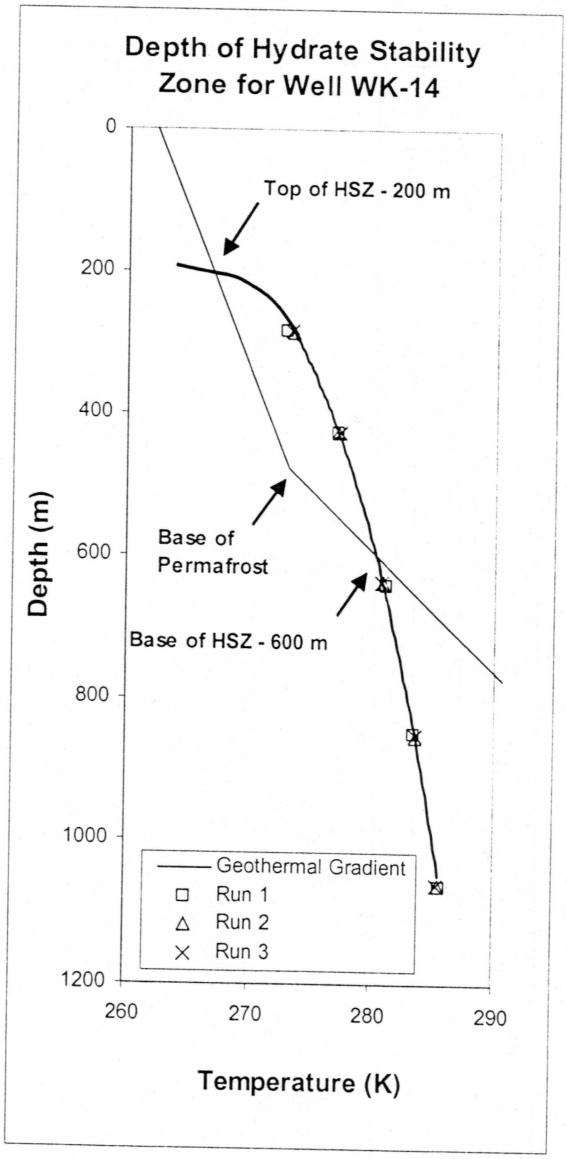

Figure 4.24: HSZ for WK-14 (2% Brine)

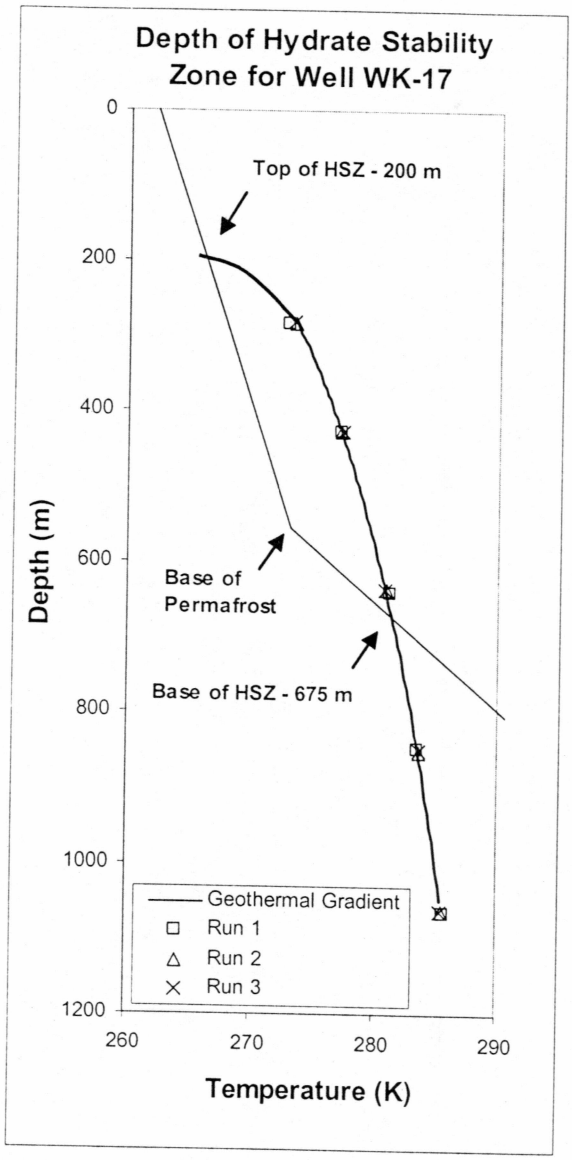

Figure 4.25: HSZ for WK-17 (2% Brine)

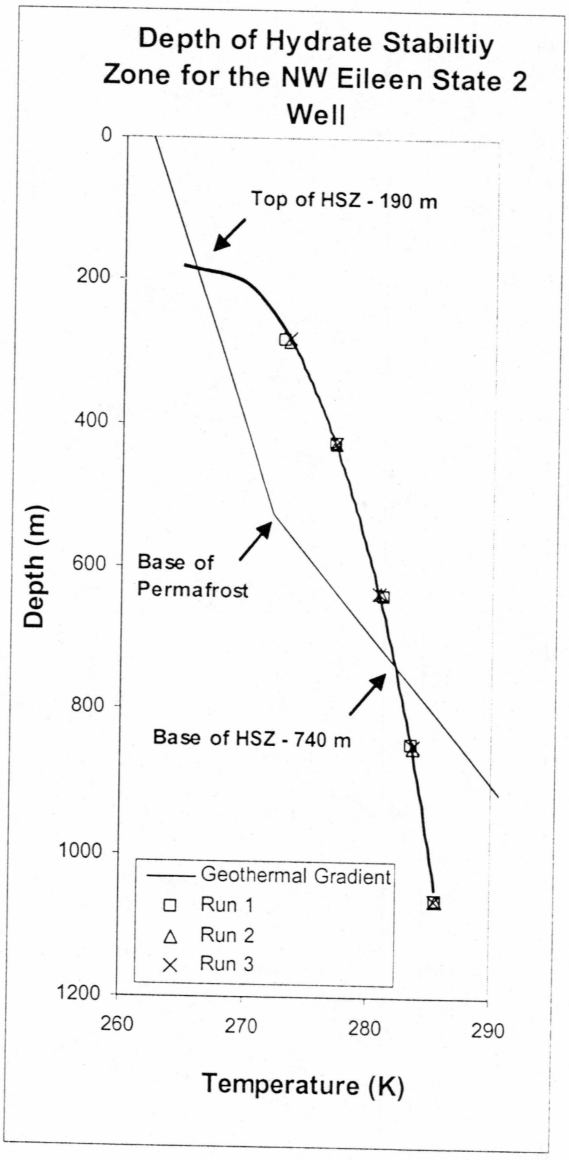

Figure 4.26: HSZ for NWEN (2% Brine)

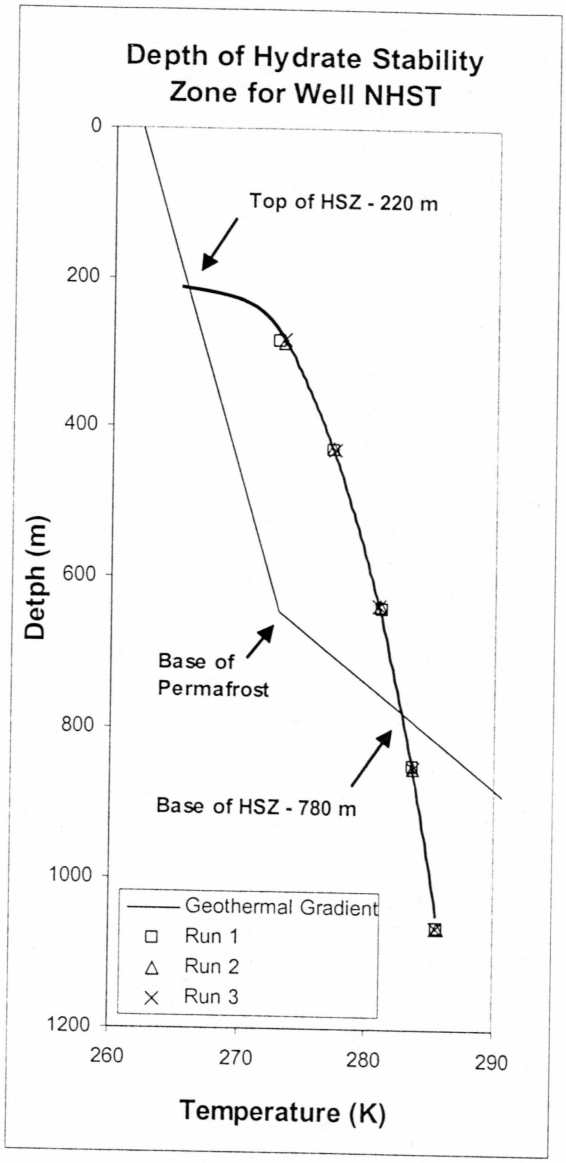

Figure 4.27: HSZ for NHST (2% Brine)

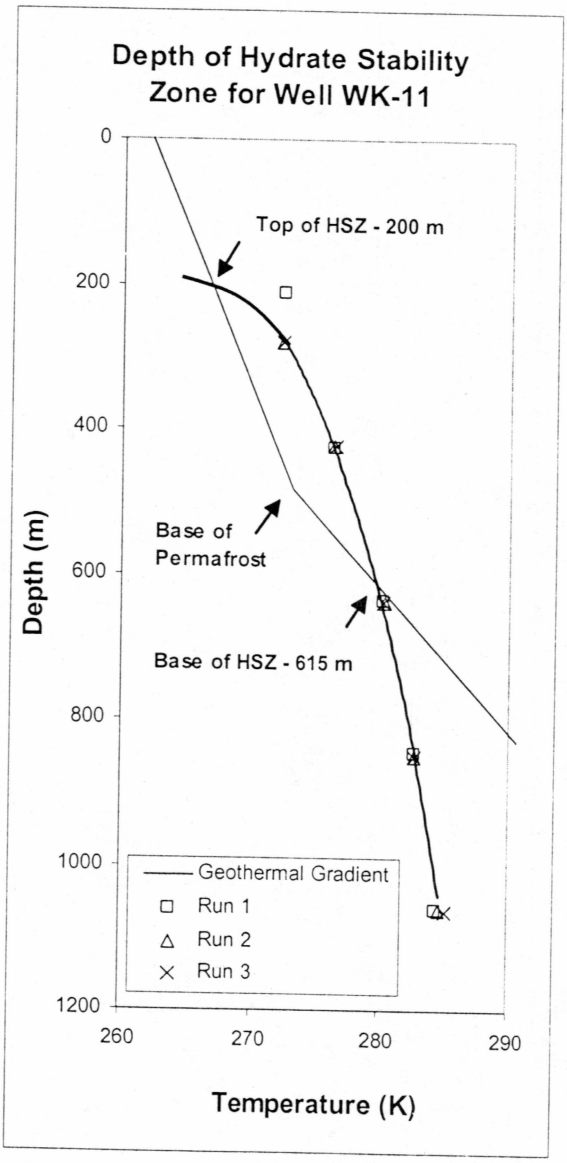

Figure 4.28: HSZ for WK-11 (4% Brine)

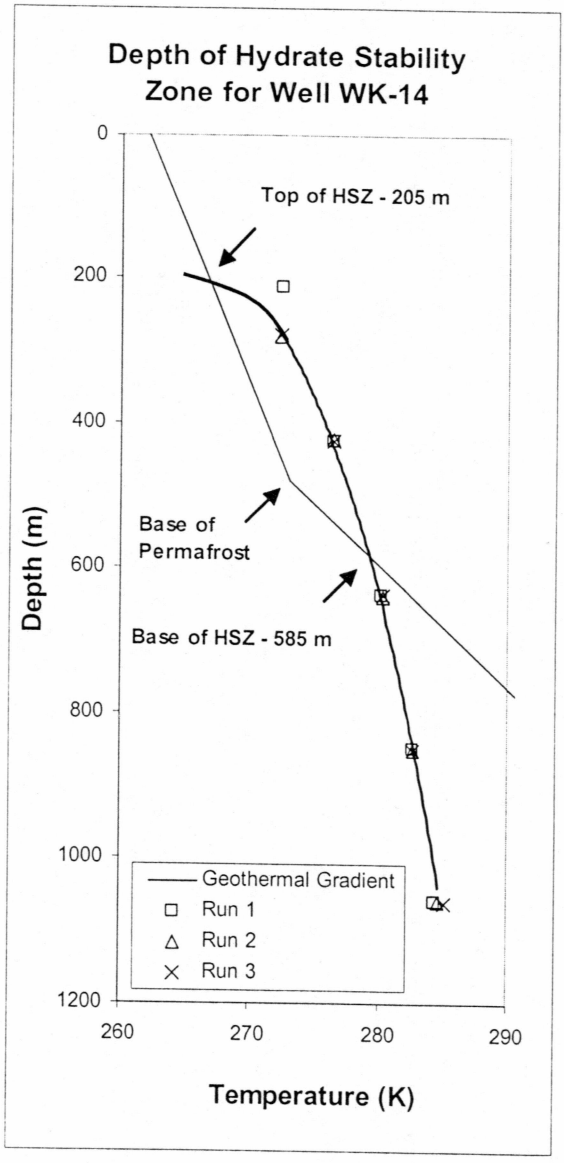

Figure 4.29: HSZ for WK-14 (4% Brine)

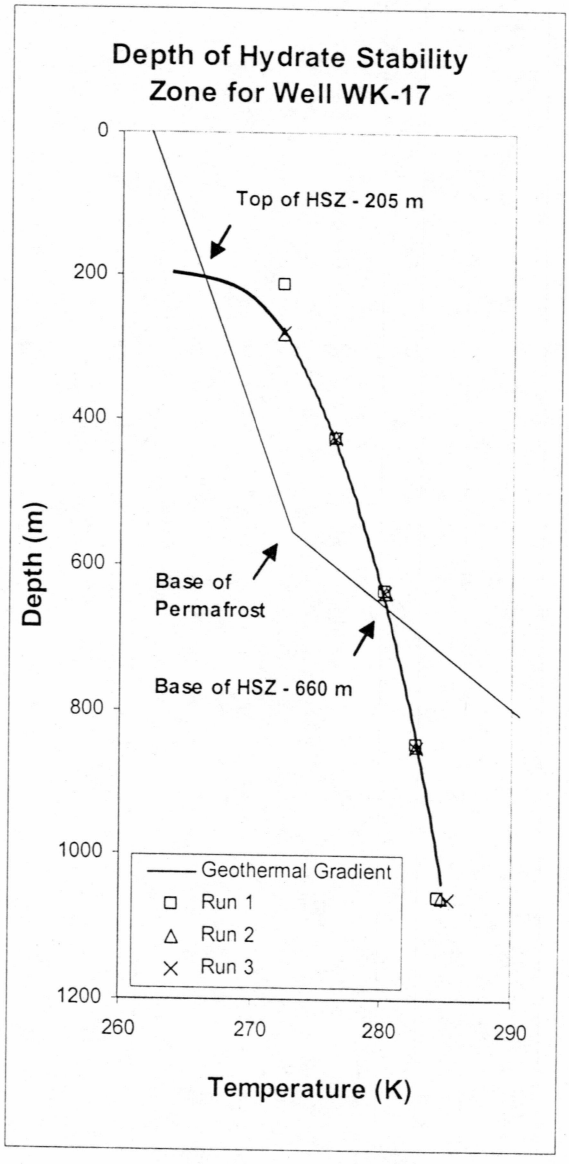

Figure 4.30: HSZ for WK-17 (4% Brine)

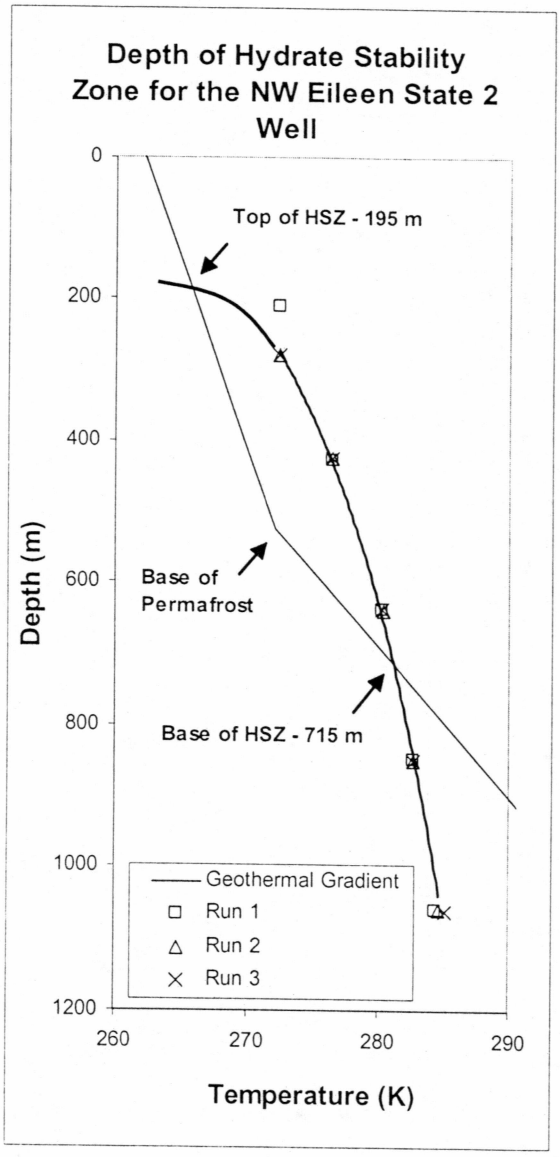

Figure 4.31: HSZ for NWEN (4% Brine)

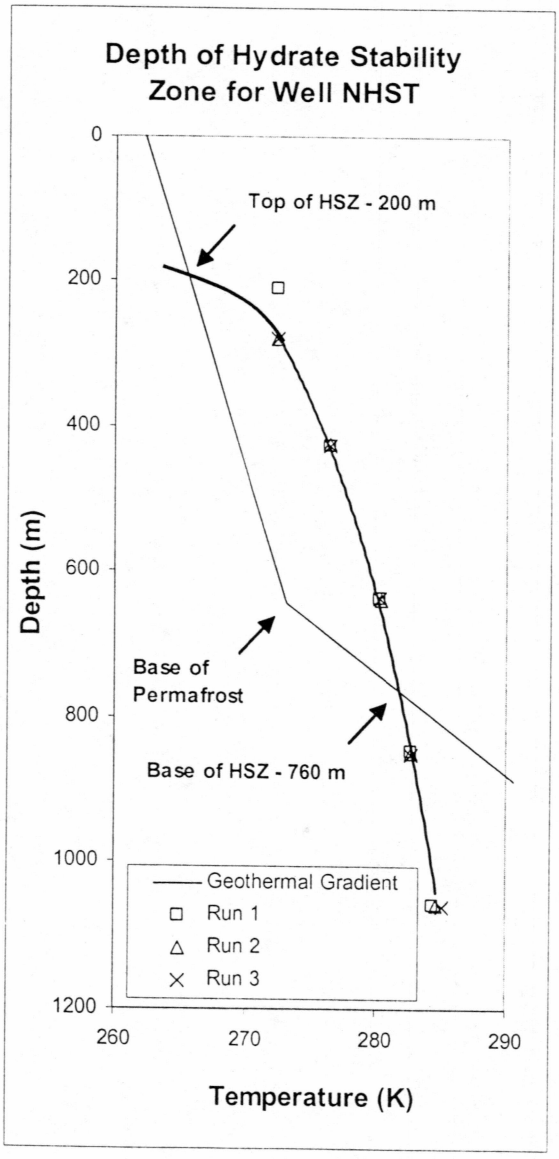

Figure 4.32: HSZ for NHST (4% Brine)

Table 4.6: Extent of the Hydrate Stability Zone for Anadarko Field Sample

2% Brine			4% Brine		
Well	Top (m)	Bottom (m)	Well	Top (m)	Bottom (m)
WK-11	205	640	WK-11	200	615
WK-14	200	600	WK-14	205	585
WK-17	200	675	WK-17	205	660
NWEN	190	740	NWEN	195	715
NHST	220	780	NHST	200	760

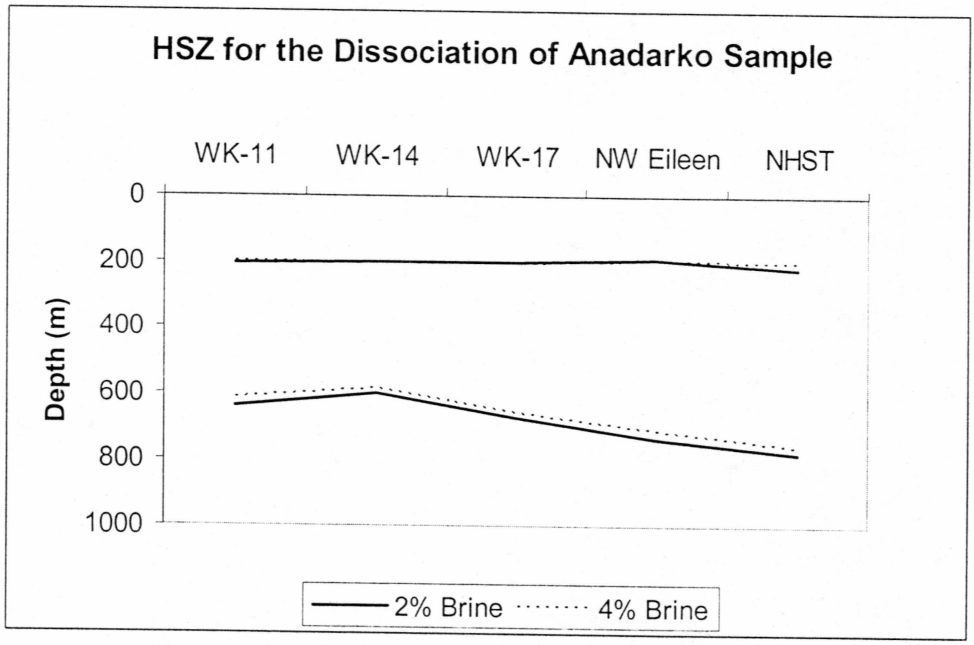

Figure 4.33: HSZ for the Anadarko Sample

The Anadarko sample showed the same general trend as the previous experiments. The HSZ increases as you move east and also increases as you move north (Figure 4.33). Table 4.6 shows the depths to the top and bottom of the hydrate stability zones. In wells WK-11, WK-14, WK-17, NWEN, and NHST the thickness of the HSZ for a 2% brine is 435, 400, 475, 550, and 560 respectively. For the 4% brine the HSZ decrease by approximately 20 to 30 meters. These hydrate stability zones are approximately 160 m less than the work conducted by Lachenbruch and others (1987) in which he assumed zero salinity.

The top of the hydrate stability zone does not vary by more than 5 m except in well NHST where it varies by 20 m, when comparing the 2% and 4% brine concentrations. Also there is very little difference in the HSZ when comparing the two porous media samples.

Again there were problems when trying to conduct experiments below 400 psia. This was also assumed be attributed to the formation/dissociation temperature being below the freezing point of water.

CHAPTER FIVE

CONCLUSIONS

5.1 Conclusions

The five wells being examined in this study show that as moving eastward the hydrate stability zone increases in thickness and depth. This is also true as moving northward (towards the Beaufort Sea). These results were all similar for each of the three experiments. Lachenbruch and others (1987) work also indicates a westward thinning of the hydrate stability zone.

Experiments conducted without the presence of porous media show that a 2% NaCl brine increase can affect the depth of the hydrate stability zone by 30 to 45 m. When a porous media is present a 2% brine increase only affects the depth of the hydrate stability zone by 20 to 30 m. This could be due to the additional pressure change involved when a porous media is present. Equation 7 relates the porosity, interfacial tension, and permeability to change in pressure. Changes in pressure will affect the P-T curve for a particular gas composition and will ultimately affect the hydrate stability zone.

In the presence of a porous media typically found on the North Slope of Alaska, the maximum depth of the hydrate stability zone was 780 m and was at the eastern most well (NHST). The minimum depth was located at the northern most well (WK-14) and had a depth of 585 m. Overall the thicknesses of the hydrate stability zone can vary by as much as 200 m in the PBU, KRU, and MPU on the North Slope of Alaska. However, it

should be noted that 99% pure methane was being used and this analysis is only valid for this gas composition. Changes in the gas composition can cause major variations in the depth of the hydrate stability zone. Much of this variation is dependent on the local variations of the geothermal gradient, gas composition, and the type of porous media in which hydrates are found.

In this study, the hydrate stability zone for the NW Eileen State 2 well ranges from 190 to 740 meters. In 1972, ARCO and Exxon recovered hydrate cores from the NW Eileen State 2 well at depths between 577 and 776 meters. From well log data, Collett (1993) has inferred that gas hydrate exist between a range of 575 and 675 meters. In all three cases, the ranges for the hydrate stability zones are in agreement. Also the hydrate stability zones determined in this study coincide with the work done by Lachenbruch and others (1987). It should also be noted that the results from this study only give possible depth zones where hydrates could exist, it doesn't necessary mean they do exist in these ranges.

5.2 Future Work

Since hydrates are usually found in hostile environments, it is very difficult to perform field tests. Most experiments are conducted in a laboratory while trying to mimic actual reservoir properties.

The results obtained in this study are for only five wells. It might be useful to analyze more wells. Comparing these results to well-log data from numerous wells could help determine where methane hydrates are most favorable to form. Also it would be

interesting to compare the results from this study to seismic surveys to see if there is any correlation between the two. The analysis in this study was for 99% methane, it could be useful to perform these experiments using different gas composition that are typically found on the North Slope of Alaska.

In order to bring this resource to the commercial market, the extent of where methane hydrates exist has to be known.

REFERENCES

1. Bradner, T., *Anadarko Petroleum Corp. Prepares Hydrate Test Next Spring*, Alaska Oil and Gas Reporter, November 12, 2002.

2. Chuvilin E.M., and Yakushev, V.S., *Structure and Some Properties of Frozen Hydrate-containing soils*, Proceedings of International Symposium on Methane Hydrates: Resources in the Near Future, JNOC-TRC, Chiba City, Japan, October 20-22, 1998.

3. Collett, T.S., *Natural Gas Hydrates-Vast Resource, Uncertain Future*, USGS Fact Sheet FS-021-01, March 2001.

4. Collett, T., *Methane Hydrate: An Unlimited Energy Resource*, Proceedings of International Symposium on Methane Hydrates: Resources in the Near Future, JNOC-TRC, Chiba City, Japan, October 20-22, 1998.

5. Collett, T.S., Gas *Hydrate Resources of Northern Alaska*, Bulletin of Canadian Petroleum Geology, v. 45, 1997, pp. 317-338.

6. Collett, T.S., *Natural Gas Hydrates of the Prudhoe Bay and Kuparuk River Area, North Slope, Alaska*, The American Association of Petroleum Geologist Bulletin, Vol. 77, No. 5,May 1993 pp. 793-812.

7. Collett, T.S., Bird, K.J., Kvenvolden, K.A., and Magoon, L.B., *Geologic Interrelations relative to gas hydrates within the North Slope of Alaska*, U.S. Geological Survey Open File Report 88-389, 1988 pp. 150.

8. Dallimore, S.R., Uchida, T., and Collett, T.S., *Scientific Results from JAPEX/JNOC/GSC Malik 2L-38 Gas Hydrate Research Well, Mackenzie Delta, Northwest Territories, Canada*, Geological Survey of Canada Bulletin 544 1999, pp. 1.

9. Godbole, S.P., Kamath, V.A., and Ehlig-Economides, C., *Natural Gas Hydrate in the Alaskan Arctic*, SPE Formation Evaluation, paper SPE 13593, March 1988, pp. 263-266.

10. Holder, G.D., Malone, R.D., and Lawson, W.F., *Effects of Gas Composition and Geothermal Properties on the Thickness and Depth of Natural-Gas-Hydrate Zones*, Journal of Petroleum Technology, paper SPE 13595, September 1987, pp. 1147-1152.

11. Kamath, A., Godbole, S.P., Ostermann, R.D., and Collett, T.S., *Evaluation of the Stability of Gas Hydrates in Northern Alaska*, Cold Regions Science and Technology, Vol. 14, No. 2, August 1987, pp. 107-119.

12. Katz, D.L., *Depths to which frozen gas fields may be expected*, Journal of Petroleum Technologies, vol. 23, April 1971, pp. 419.

13. Klauda, J.B., and Sandler, S.I., *Modeling Gas Hydrate Phase Equilibria in Laboratory and Natural Porous Media*, Ind. Eng. Chem. Res., Vol. 40, 2001, pp. 4197-4208.

14. Kvenvolden, K.A., *Estimates of the Methane Content of Worldwide Gas-Hydrate Deposits*, Proceedings of International Symposium on Methane Hydrates: Resources in the Near Future, JNOC-TRC, Chiba City, Japan, October 20-22, 1998.

15. Kvenolden, K.A., *Methane Hydrate-A Major Reservoir of Carbon in the Shallow Geosphere*, Chemical Geology 71, 41, 1988.

16. Kvenvolden, K.A. and McMenamin, M.A., *Hydrates of Natural Gas: A Review of Their Geologic Occurrence*, U.S. Geological Survey Circular 825, 1980.

17. Lachenbruch, A.H., Galanis Jr., S.P., and Moses Jr., T.H., *A Thermal Cross Section for the Permafrost and Hydrate Stability Zones in the Kuparuk and*

Prudhoe Bay Oil Fields, Geologic Studies in Alaska by the U.S. Geological Survey during 1987, 1988, pp. 48-51.

18. Makogon, Y.F., *Hydrates of Natural Gas*, Penn Well Publishing Company, Tulsa, Oklahoma, 1981, pp. 2-4.

19. Marshall, B.V., Munroe, R.J., Kennelly, Jr., J.P., Galanis, Jr., S.P., and Moses, Jr., T.H., *Temperature and Depth of Permafrost on the Alaskan Arctic Slope*, The Alaska Geological Society, Anchorage, Alaska, October 1987.

20. Osterkamp, T. E., and Payne, M.W., *Estimates of Permafrost thickness from well logs in northern Alaska*, Cold Regions Science and Technology, v.5, 1981, pp. 13-27.

21. Ripmeester, J.A., Tse, J.S., Ratcliffe, C.I., and Powell, B.M., *A New Clathrate Hydrate Structure*, Nature, v. 325, 1987, pp. 135.

22. Sloan Jr., D.E., *Hydrate Engineering*, Society of Petroleum Engineers, Richardson, Texas, 2000, pp. 63-67.

23. Smosna, R.A., and Mroz, T.H., *Petrographic Characterization of Hydrate Reservoirs in Northern Alaska*, The Third Chemical Congress of North America, Toronto, Canada, 1988.

24. USGS Website, *U.S. Geological Survey's Borehole Temperature Logs from Arctic Alaska, pre-1989*, http://climchange.cr.usgs.gov/data/bht/alaska.

25. Valin, Z.C., Collett, T.S., *Molecular and Isotopic Analyses of the Hydrocarbon Gases Within Gas Hydrate-Bearing Rock Units of the Prudhoe Bay-Kuparuk River Area in Northern Alaska*, U.S. Geological Survey Open-File Report 92-299, 1992, pp. 1-13.

26. Van Der Waals, J.H. and Platteeuw, J.C. *Clathrate Solutions*, Advances in Chemical Physics, Vol. 2, 1959, pp. 2-10.

27. Vasillev, V.G., Makagon, Y.F., Trebin, F.A. et al., *Otkrytiya, izobreteniya, promyshlennye obraztsy, tovarnyo znakl (Discoveries, Inventions, Industrial Samples, Trademarks)*, (Moscow: TsNHPI,) 10, 4 (in Russian), 1970.

28. Winters, W.J., Waite, W.F., Mason, D.H., Dillon, W.P., Pecher, I.A., *Sediment Properties Associated With Gas Hydrate Formation*, Proceedings of the Fourth

International Conference on Gas Hydrates, Yokohama, May 19-23, 2002, pp. 722-727.

29. Youslf, M.H., Abass, H.H., Selim, M.S., and Sloan, E.D., *Experimental and Theoretical Investigation of Methane-Gas-Hydrate Dissociation in Porous Media*, SPE Reservoir Engineering, Paper SPE 19320, February 1991, pp. 69-76.

30. Yousif, M.H. and Sloan, E.D., *Experimental Investigation of Hydrate Formation and Dissociation in Consolidated Porous Media*, SPE Reservoir Engineering, November 1991, pp. 452-458.

31. Zhang, W., and Smith D.H., "Constructing Thermodynamic Equations for Ice-Hydrate Equilibria in Porous Media", In-house DOE Report, 2003.

32. Zhang, W., Wilder, J.W., and Smith, D.H., *Equilibrium Pressures and Temperatures for Equilibria Involving Hydrate, Ice, and Free Gas in Porous Media*, Proceeding from the 4th International Conference on Gas Hydrates, Yokohama, May 19-23, 2002.

APPENDIX A

SAPPHIRE CELL HYDRATE DISSOCIATION

1500 psia, 2% Brine Solution

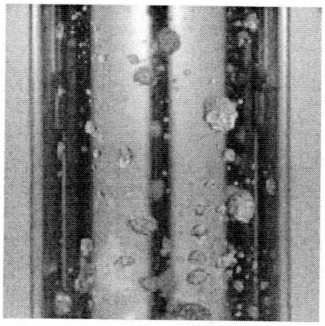

Figure A1: 54.3 °F, 0 min

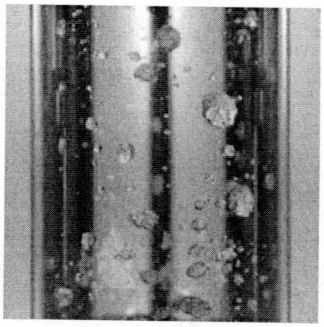

Figure A2: 54.3 °F, 0.5 min

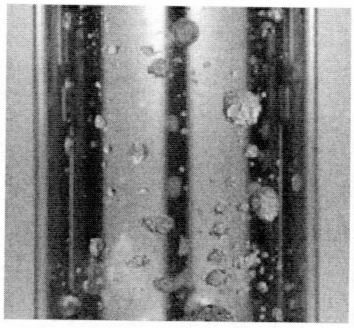

Figure A3: 54.3 °F, 1 min

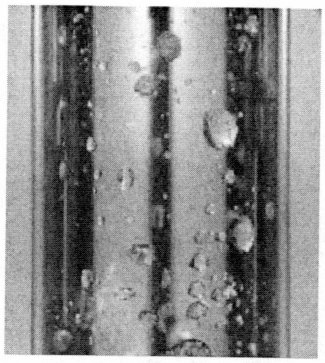

Figure A4: 54.4 °F, 1.5 min

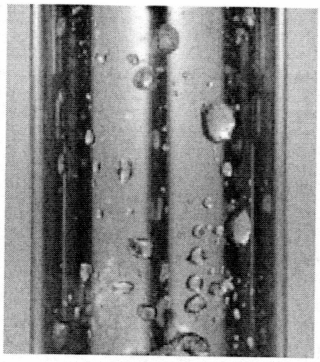

Figure A5: 54.4 °F, 2 min

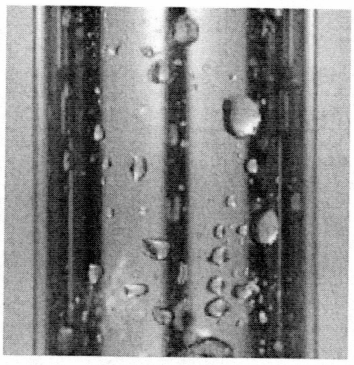

Figure A6: 54.5 °F, 2.5 min

1200 psia, 2% Brine Solution

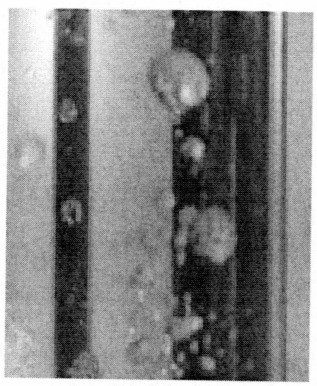

Figure A7: 51.3 °F, 0 min

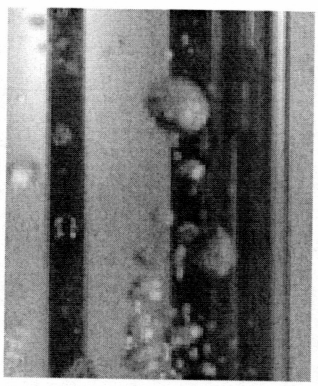

Figure A8:51.3 °F, 0.5 min

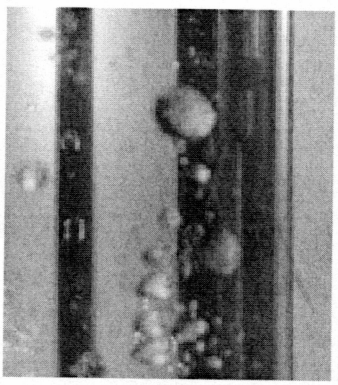

Figure A9: 51.3 °F, 1 min

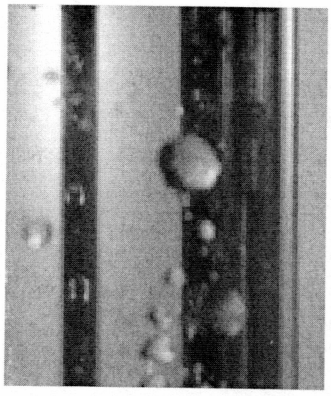

Figure A10: 51.4 °F, 1.5 min

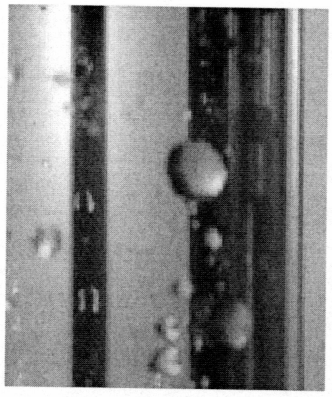

Figure A11: 51.4 °F, 2 min

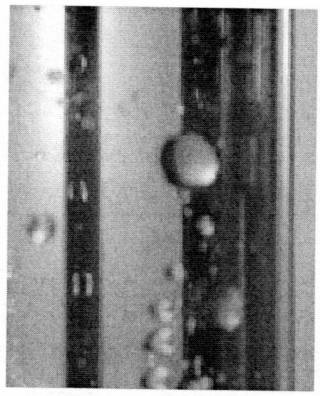

Figure A12: 51.5 °F, 2.5 min

900 psia, 2% Brine Solution

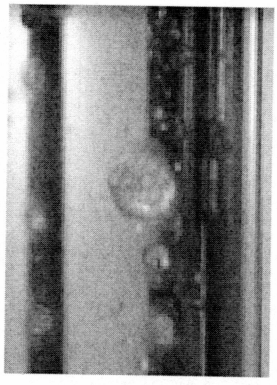

Figure A13: 49 °F, 0 min

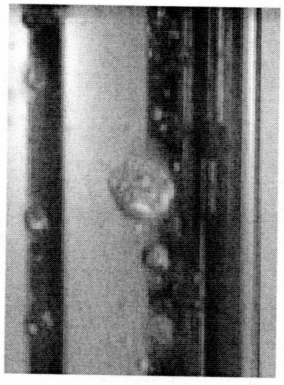

FigureA14: 49.2 °F, 0.5 min

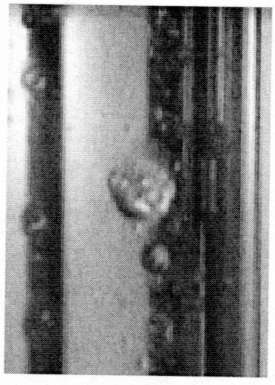

Figure A15: 49.1 °F, 1 min

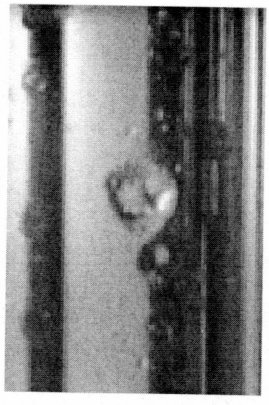

Figure A16: 49.3 °F, 1.5 min

Figure A17: 49.2 °F, 2 min

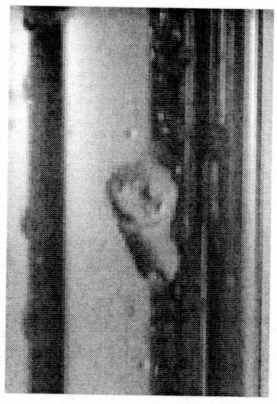

Figure A18: 49.3 °F, 2.5 min

600 psia, 2% Brine Solution

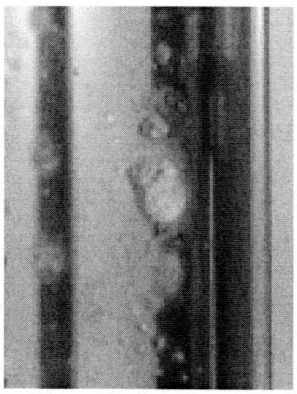

Figure A19: 42.6 °F, 0 min

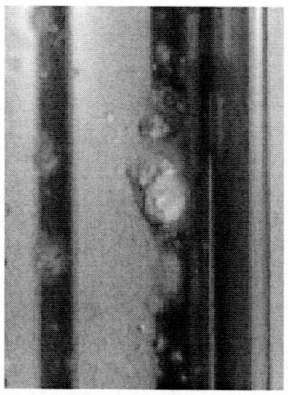

Figure A20: 42.8 °F, 2 min

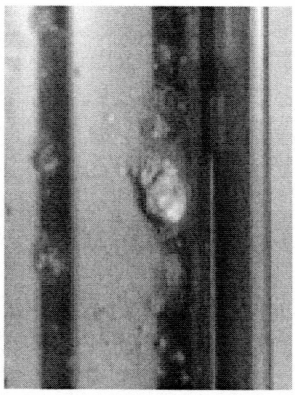

Figure A21: 42.8 °F, 4 min

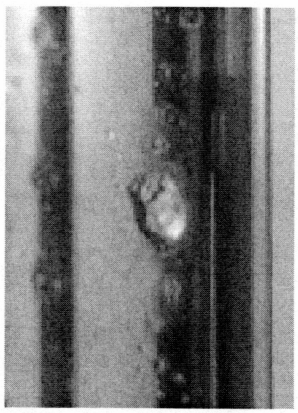

Figure A22: 42.8 °F, 6 min

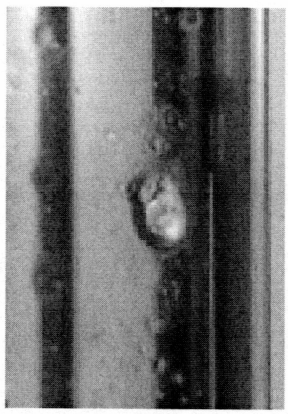

Figure A23: 42.8 °F, 8 min

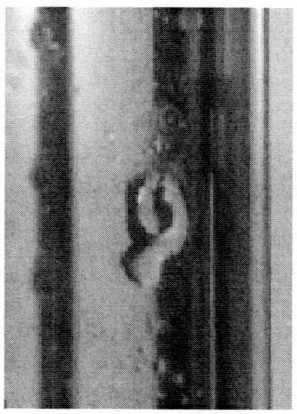

Figure A24: 42.9 °F, 10 min

300 psia, 2% Brine Solution

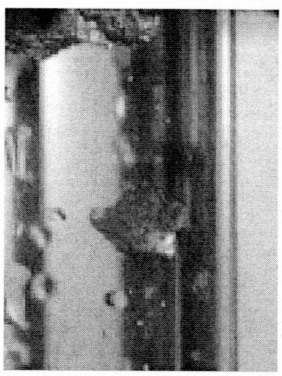

Figure A25: 29.5 °F, 0 min

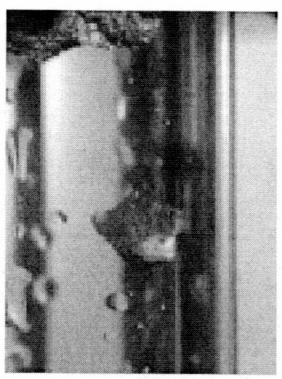

Figure A26: 29.6 °F, 2 min

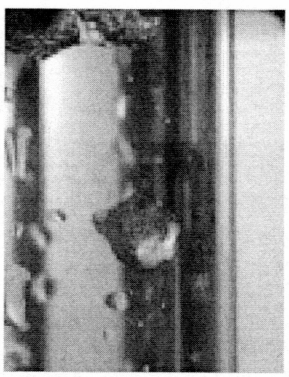

Figure A27: 29.6 °F, 4 min

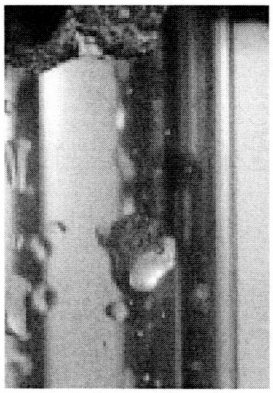

Figure A28: 29.7 °F, 6 min

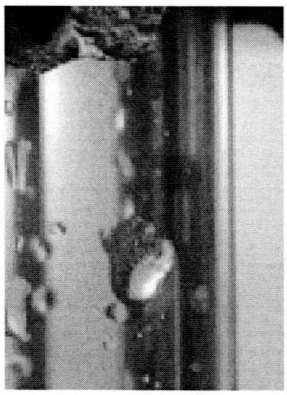

Figure A29: 29.8 °F, 8 min

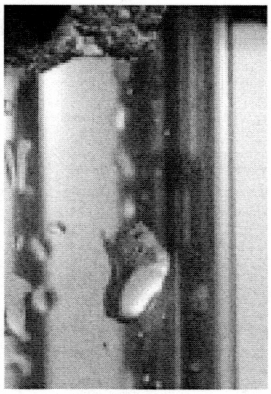

Figure A30: 29.8 °F, 10 min

1500 psia, 4% Brine Solution

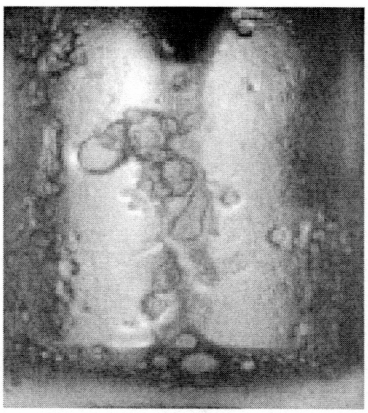

Figure A31: 52.5 °F, 0 min

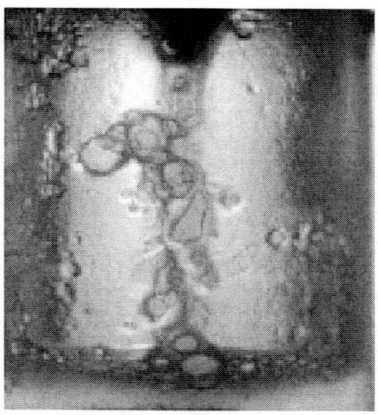

Figure A32: 52.5 °F, 5 min

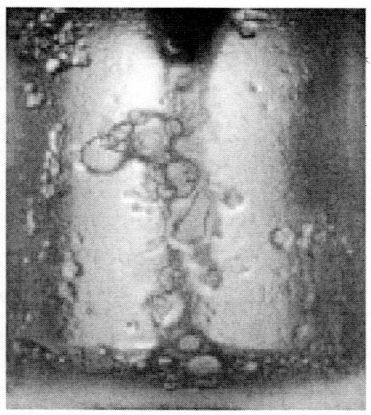

Figure A33: 52.6 °F, 10 min

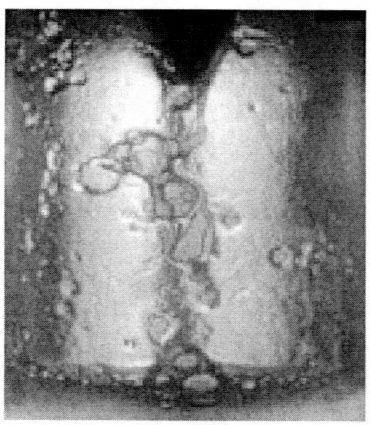

Figure A34: 52.6 °F, 15 min

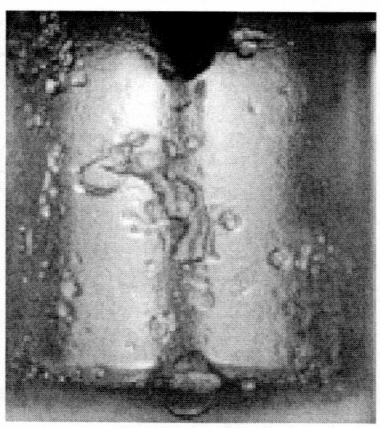

Figure A35: 52.7 °F, 20 min

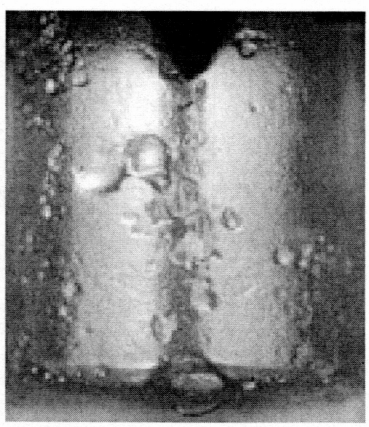

Figure A36: 52.7 °F, 25 min

1200 psia, 4% Brine Solution

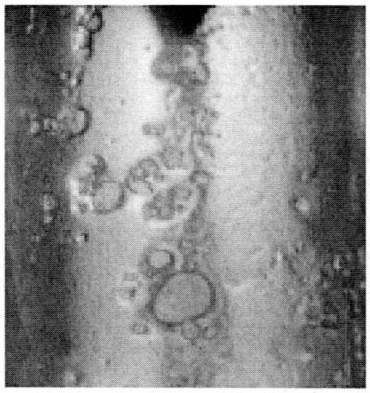

Figure A36: 48.6 °F, 0 min

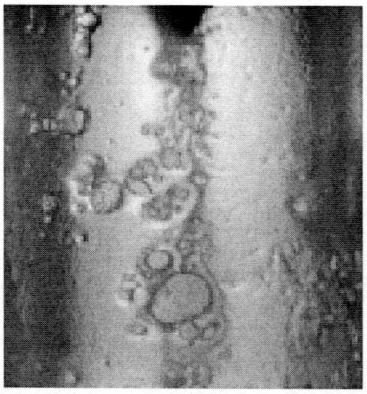

Figure A37: 48.8 °F, 5 min

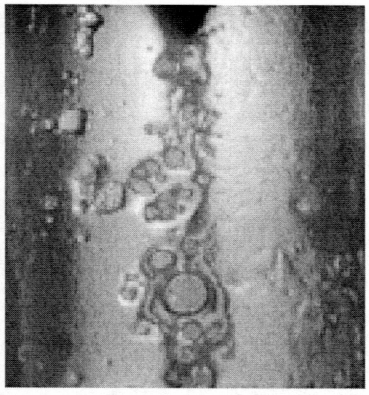

Figure A38: 48.8 °F, 10 min

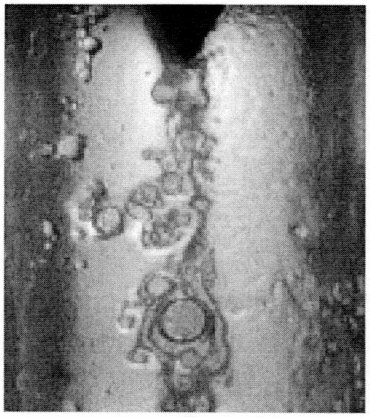

Figure A39: 48.9 °F, 15 min

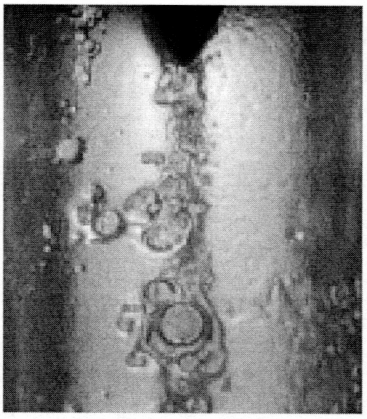

Figure A40: 49.0 °F, 20 min

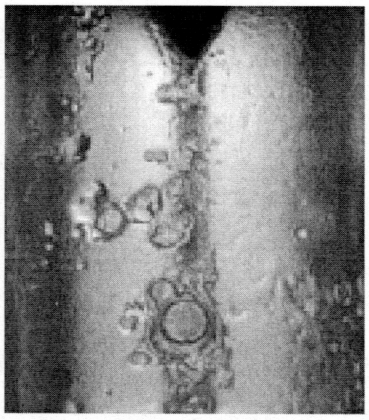

Figure A41: 49.1 °F, 25 min

900 psia, 4% Brine Solution

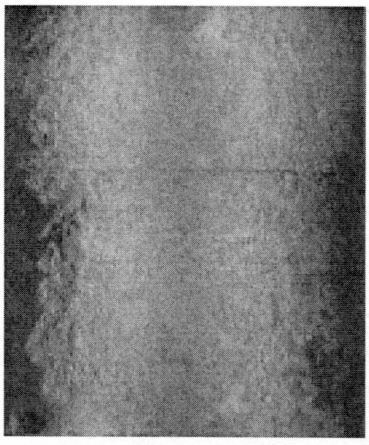

Figure A42: 43.9 °F, 0 min

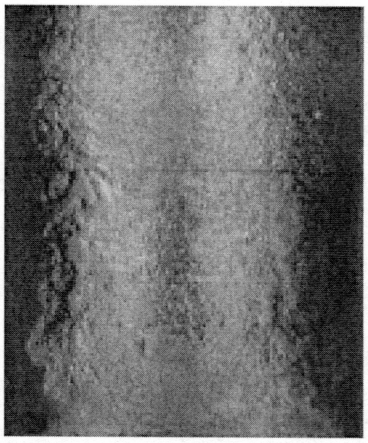

Figure A43: 44.1 °F, 5 min

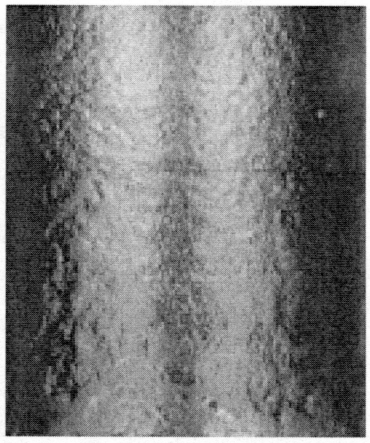

Figure A44: 44.1 °F, 10 min

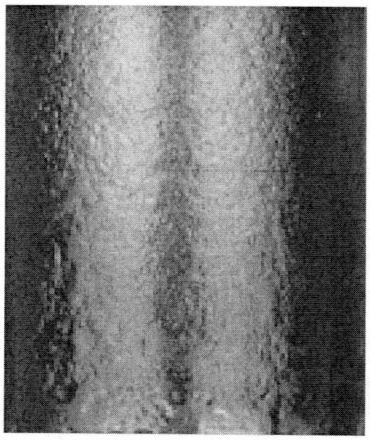

Figure A45: 44.1 °F, 15 min

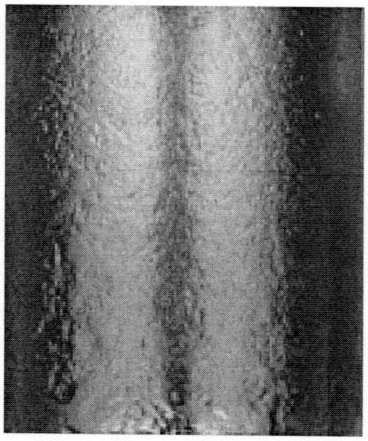

Figure A46: 44.3 °F, 20 min

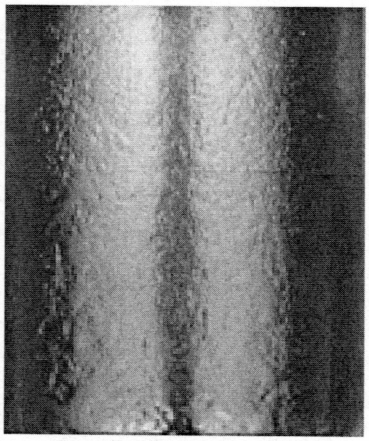

Figure A47: 44.3 °F, 25 min

600 psia, 4% Brine Solution

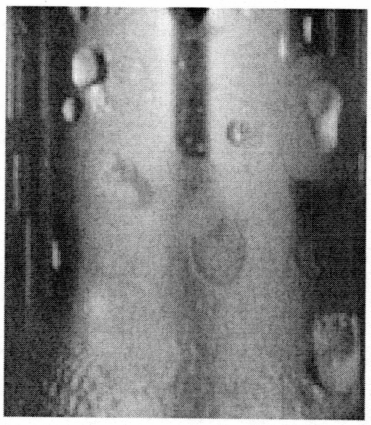

Figure A48: 37.1 °F, 0 min

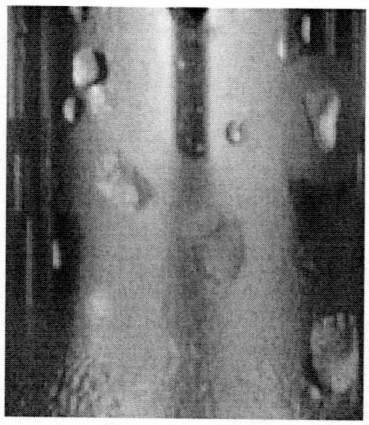

Figure A49: 37.2 °F, 2 min

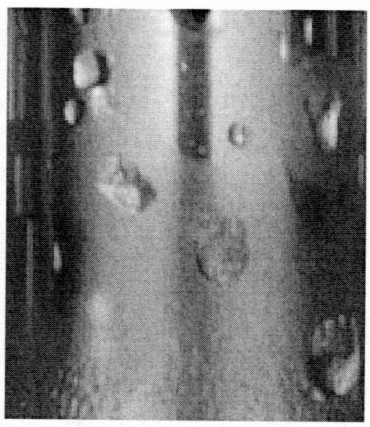

Figure A50: 37.4 °F, 4 min

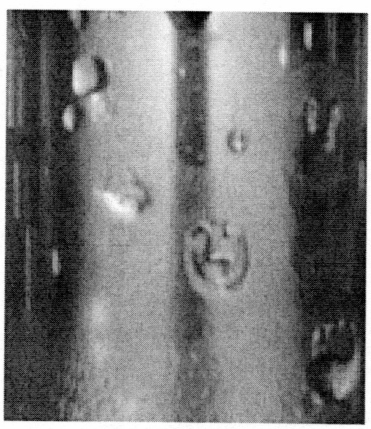

Figure A51: 37.5 °F, 6 min

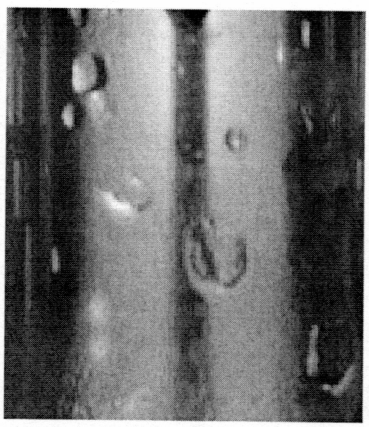

Figure A52: 37.6 °F, 8 min

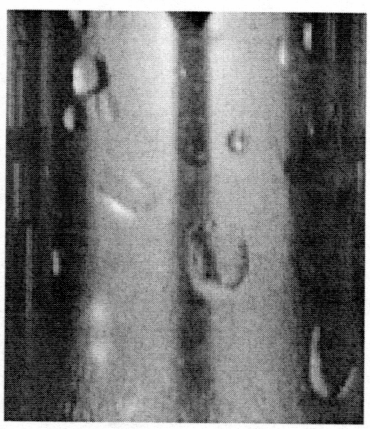

Figure A53: 37.8 °F, 10 min

300 psia, 4% Brine Solution

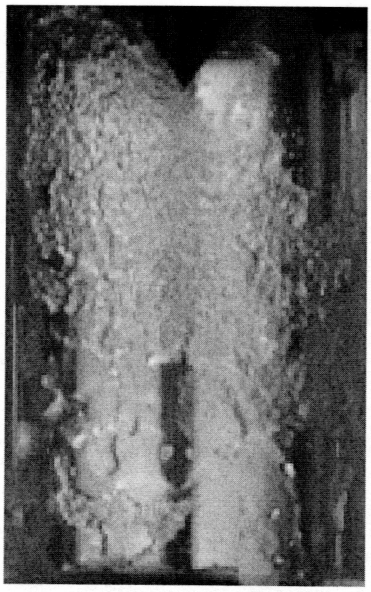

Figure A54: 27.2 °F, 0 min

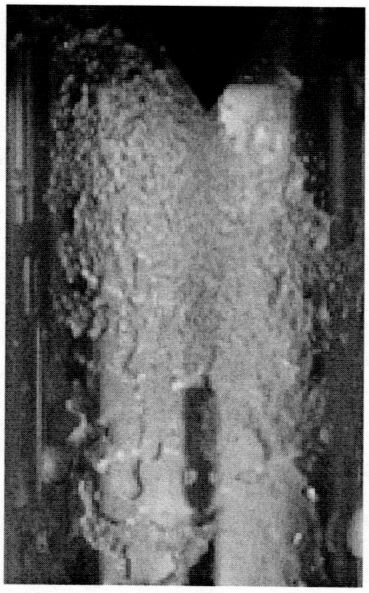

Figure A55: 27.4 °F, 2 min

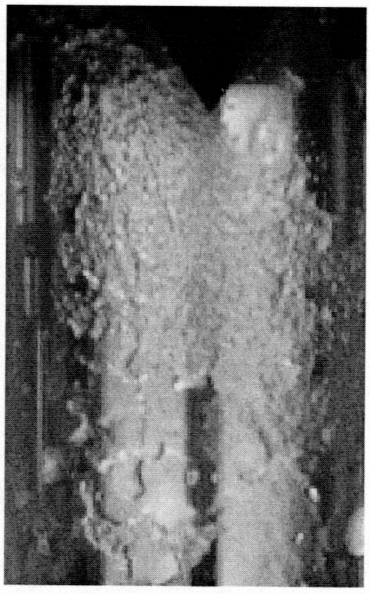

Figure A56: 27.5 °F, 4 min

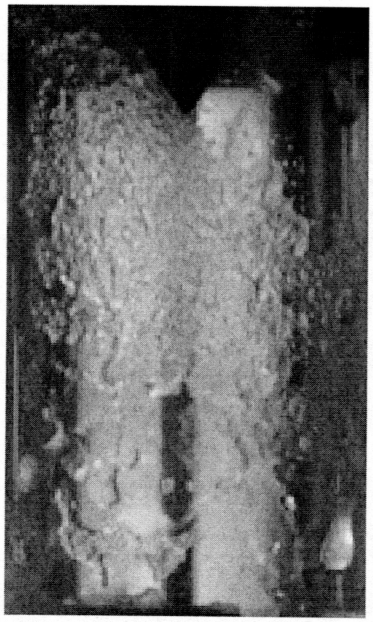

Figure A57: 27.5 °F, 6 min

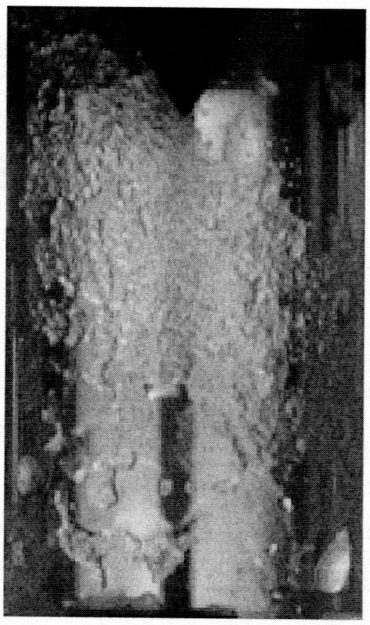

Figure A58: 27.5 °F, 8 min

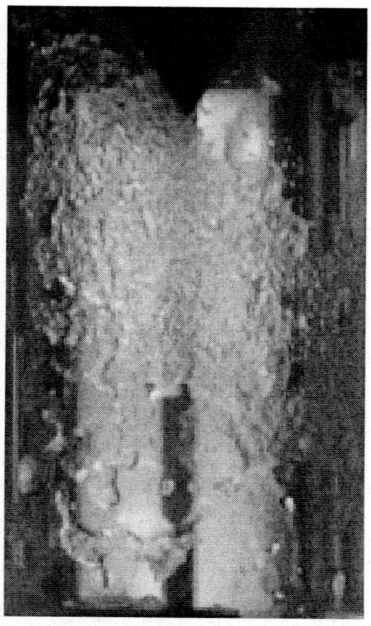

Figure A59: 27.7 °F, 10 min

APPENDIX B

HYDRATE DISSOCIATION IN A SYNTHETIC POROUS MEDIA

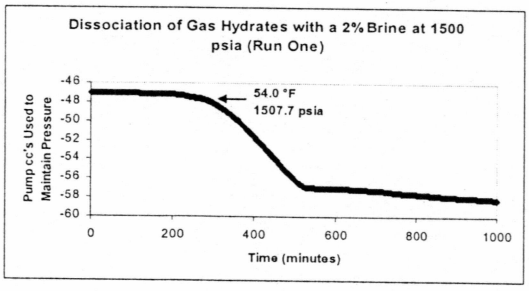

Figure B1

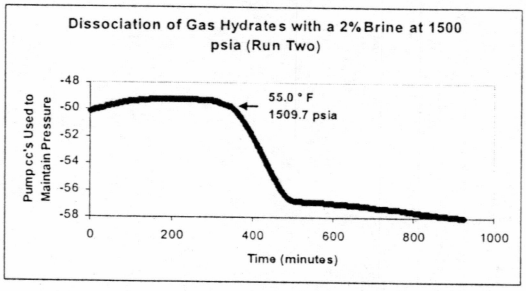

Figure B2

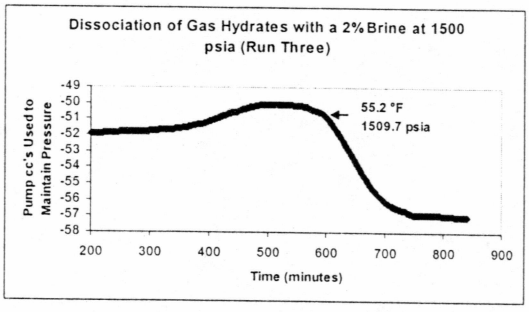

Figure B3

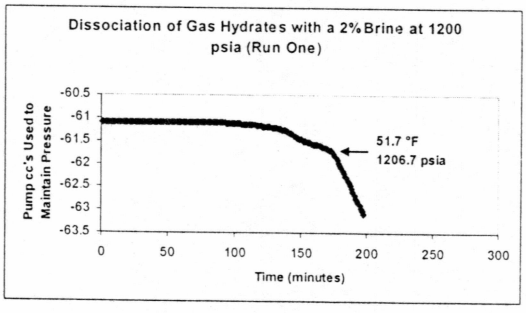

Figure B4

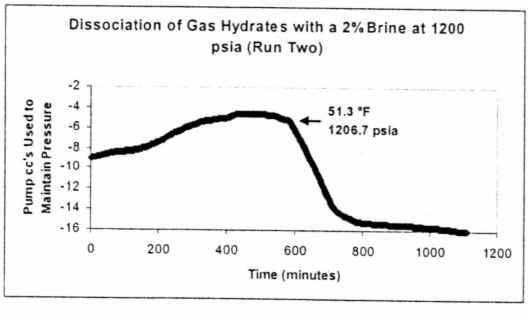

Figure B5

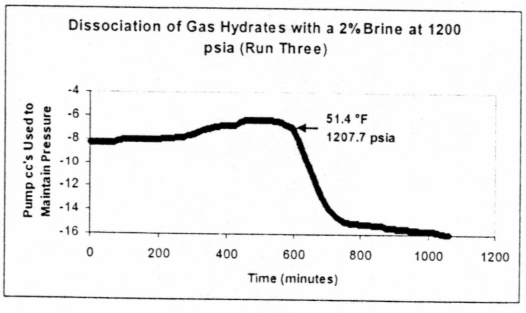

Figure B6

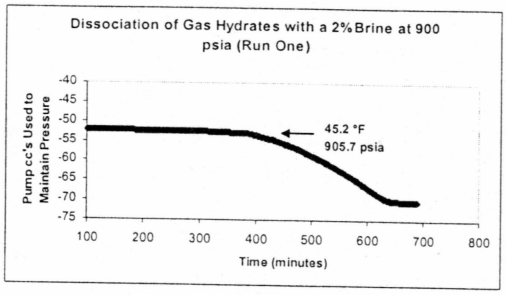

Figure B7

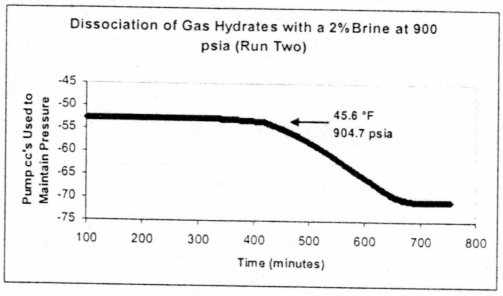

Figure B8

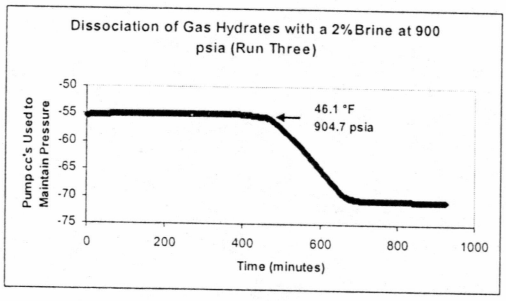

Figure B9

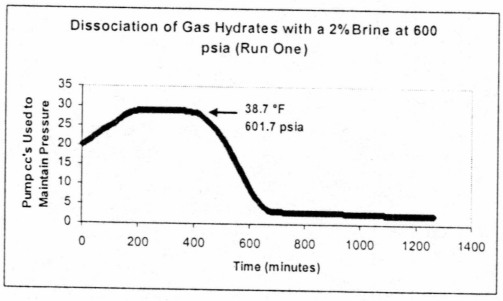

Figure B10

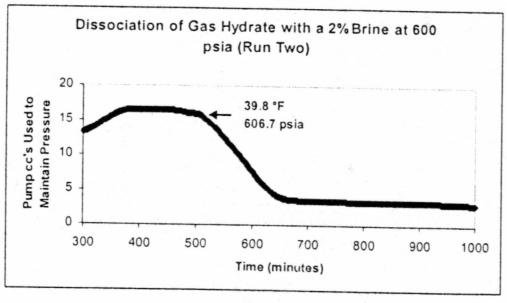

Figure B11

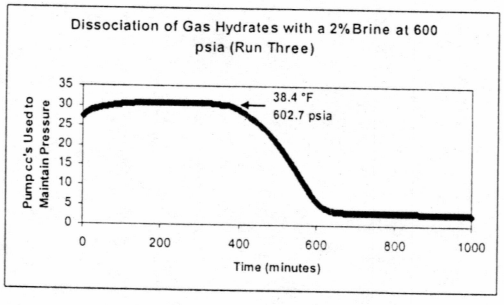

Figure B12

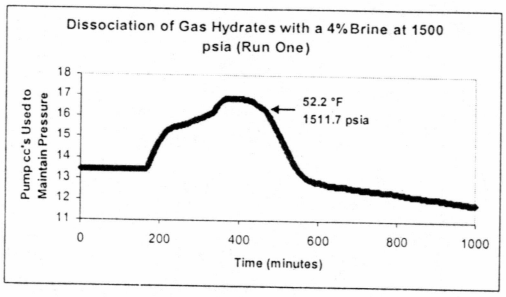

Figure B13

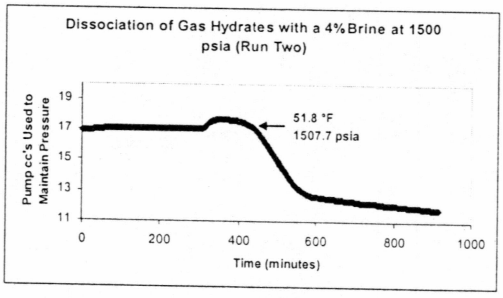

Figure B14

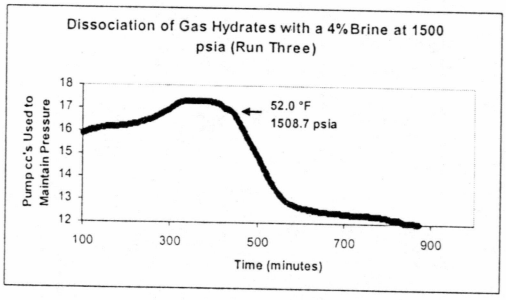

Figure B15

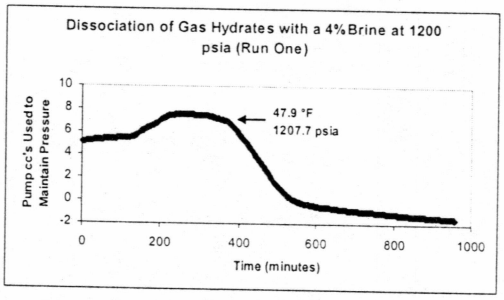

Figure B16

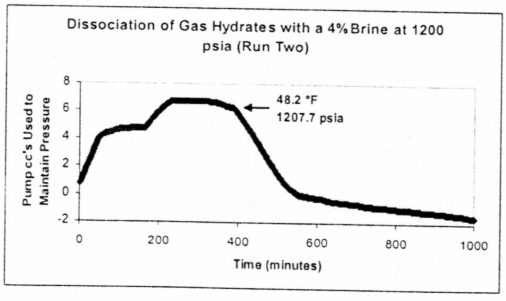

Figure B17

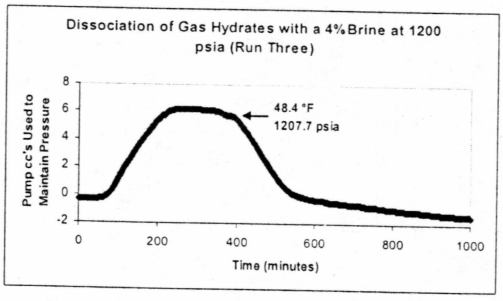

Figure B18

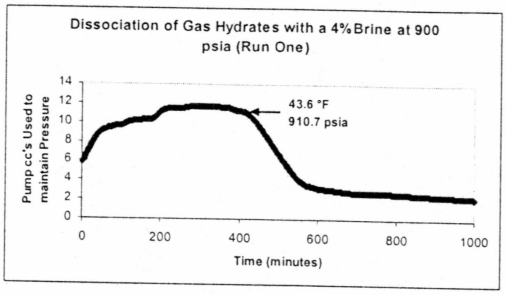

Figure B19

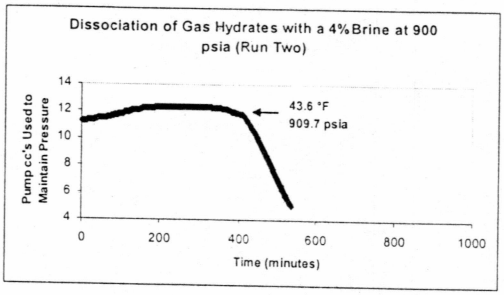

Figure B20

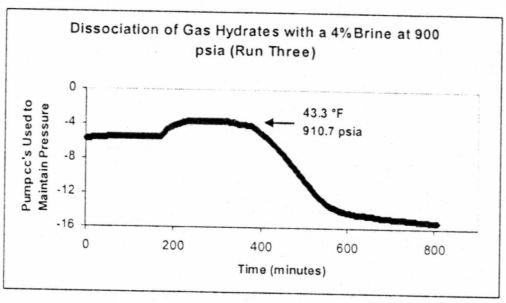

Figure B21

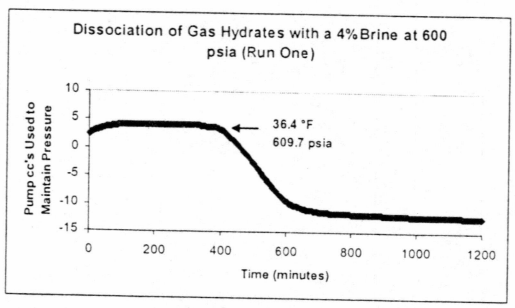

Figure B22

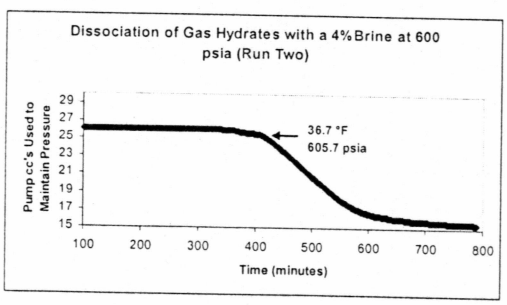

Figure B23

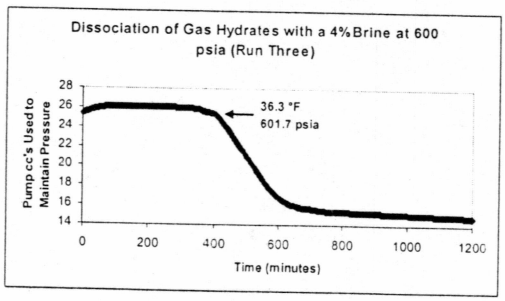

Figure B24

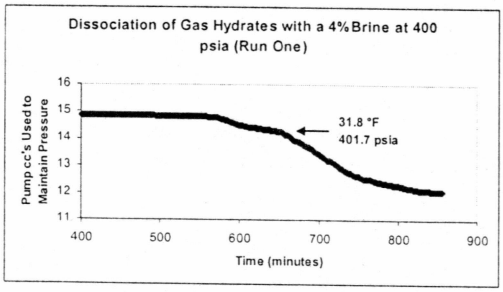

Figure B25

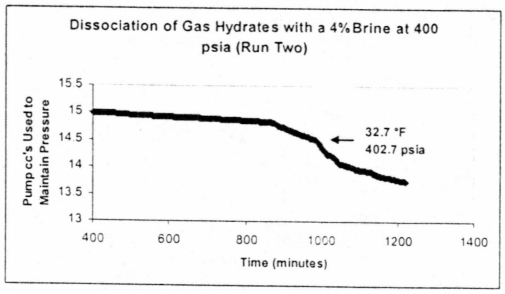

Figure B26

APPENDIX C

HYDRATE DISSOCIATION IN ANADARKO FIELD SAMPLE

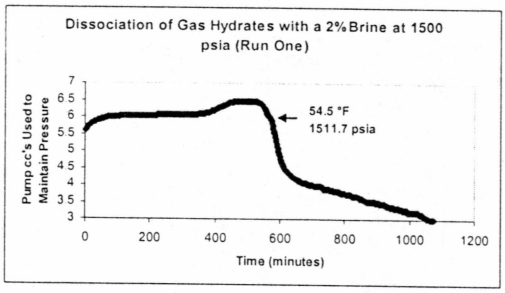

Figure C1

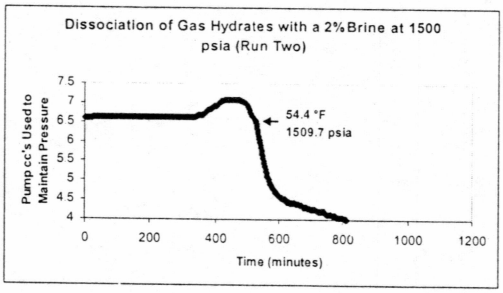

Figure C2

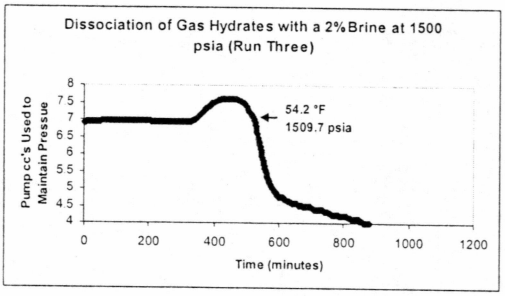

Figure C3

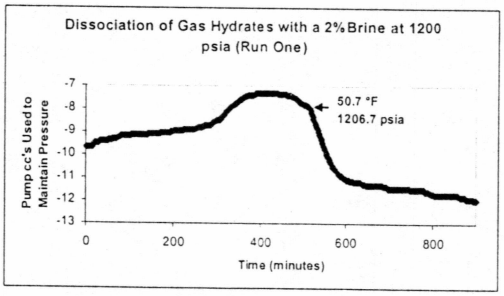

Figure C4

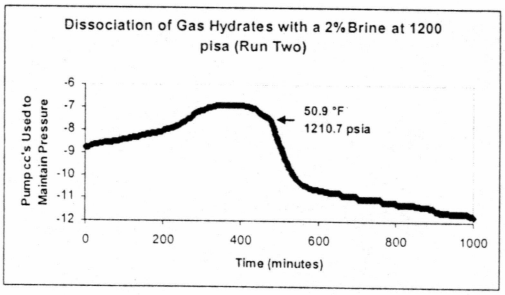

Figure C5

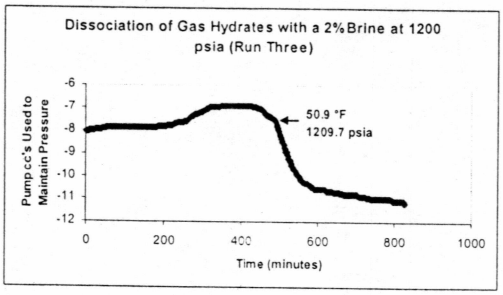

Figure C6

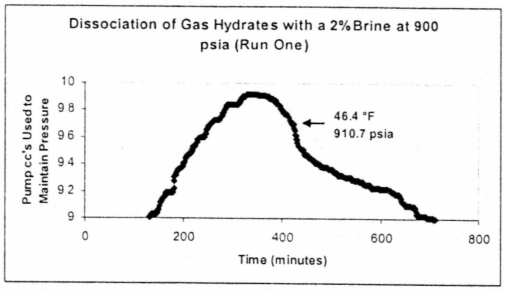

Figure C7

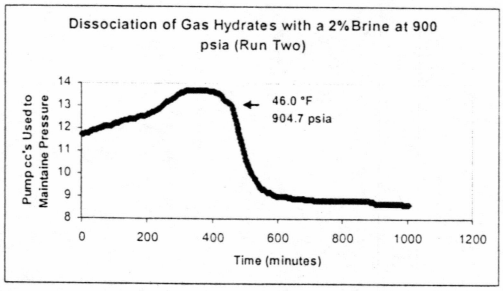

Figure C8

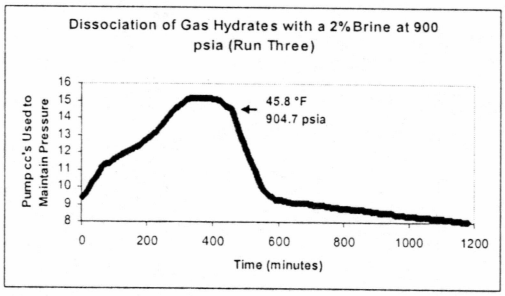

Figure C9

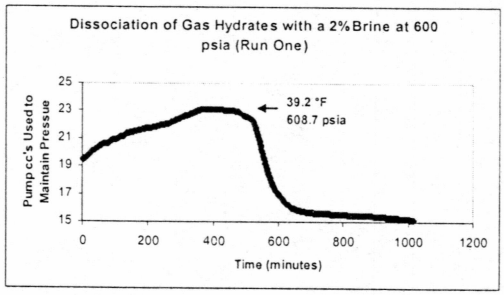

Figure C10

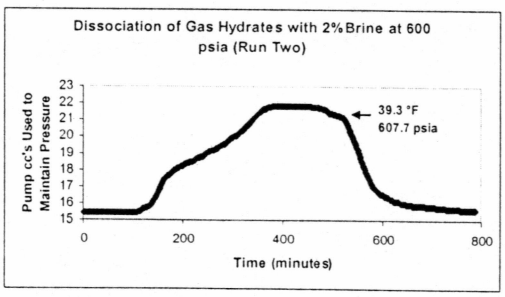

Figure C11

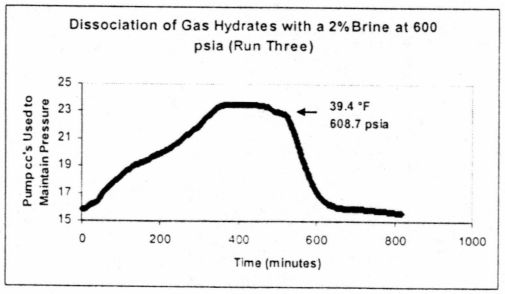

Figure C12

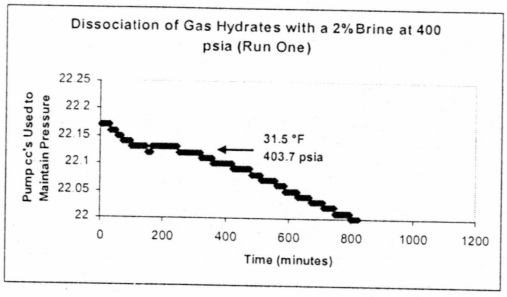

Figure C13

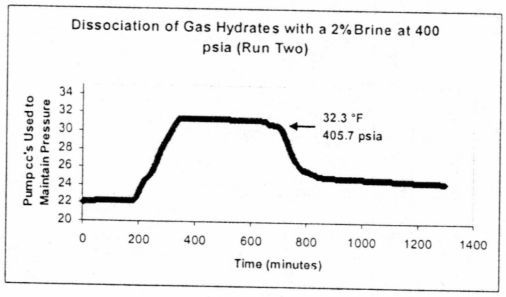

Figure C14

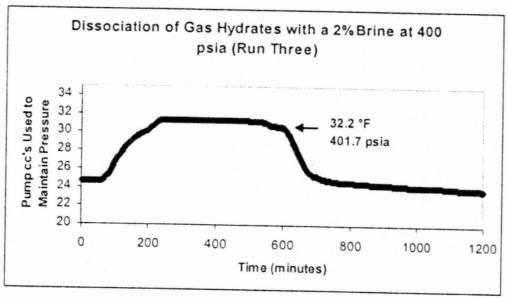

Figure C15

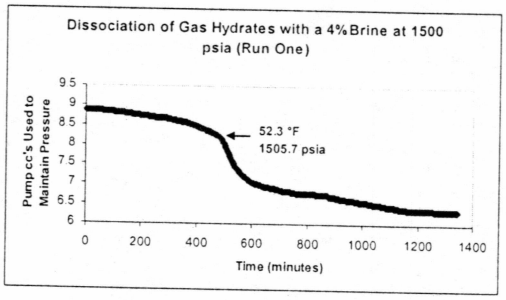

Figure C16

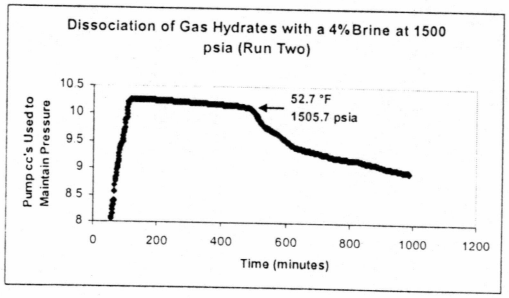

Figure C17

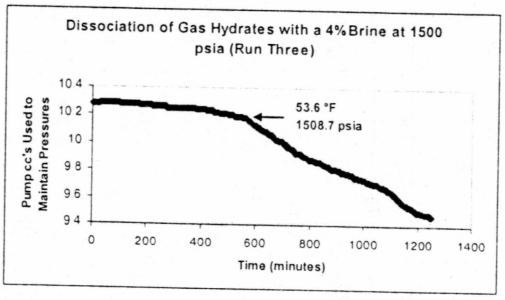

Figure C18

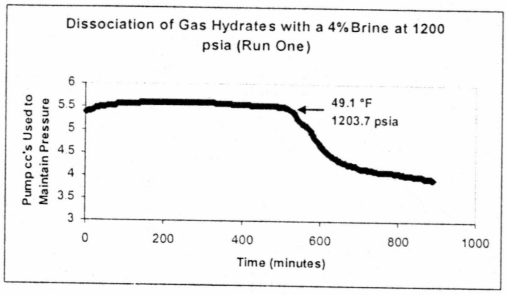

Figure C19

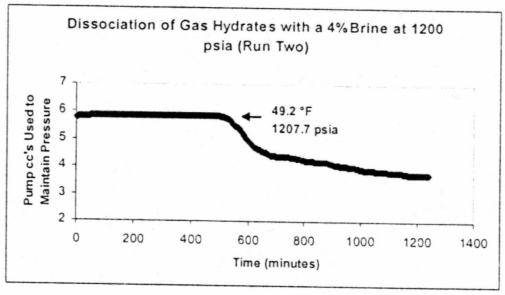

Figure C20

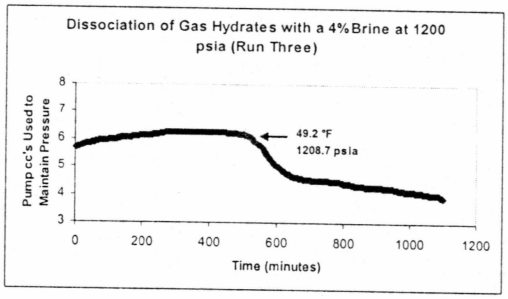

Figure C21

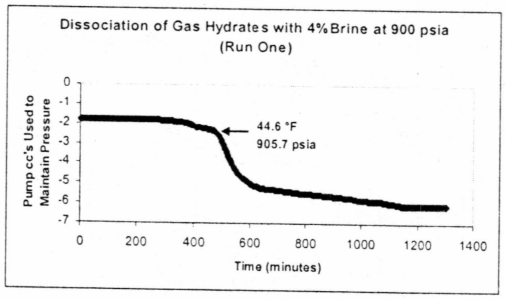

Figure C22

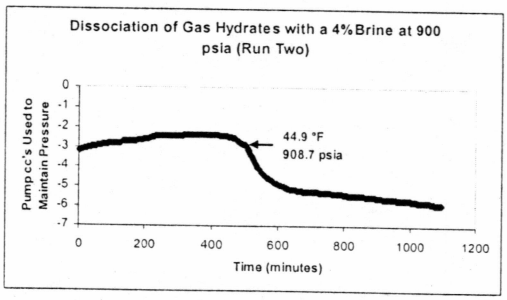

Figure C23

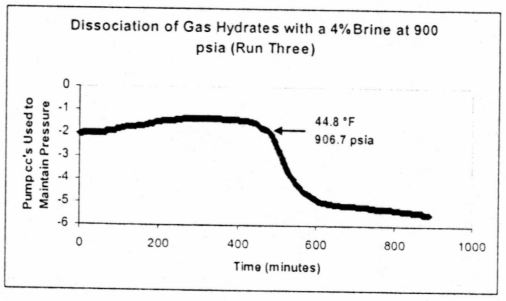

Figure C24

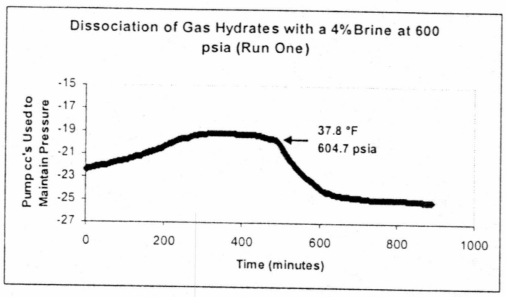

Figure C25

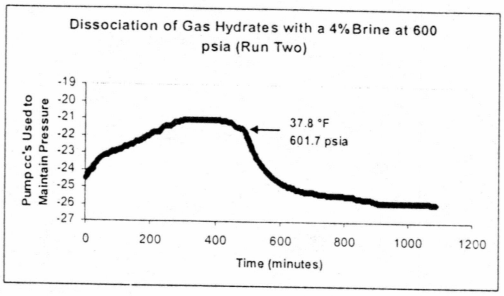

Figure C26

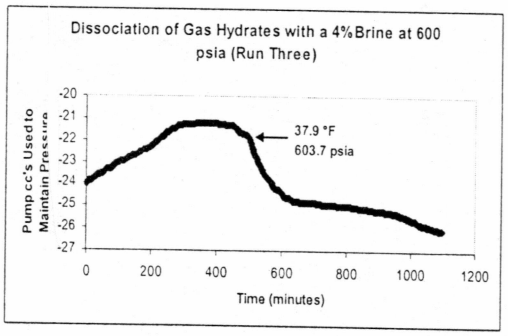

Figure C27

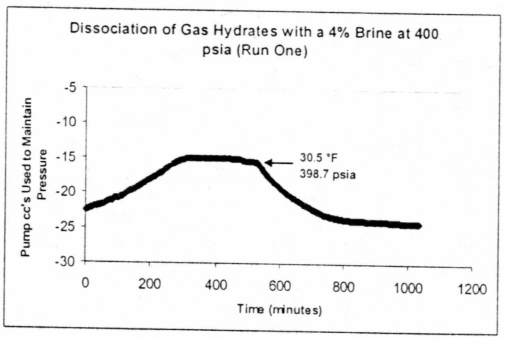

Figure C28

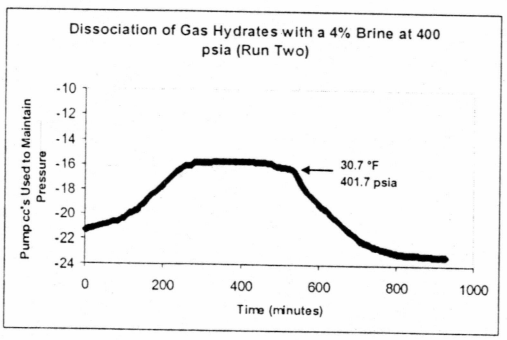

Figure C29

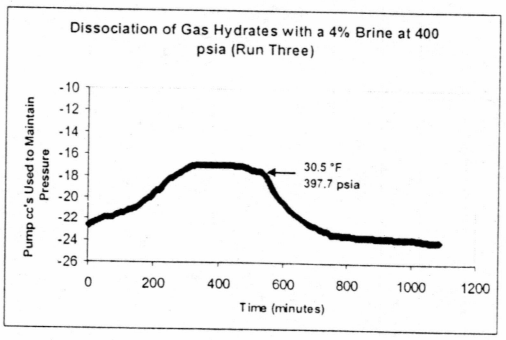

Figure C30